Spectrin coordinates cortical actomyosin organization and differentiation essential for a functional epithelial barrier

Arad Soffer[1]*, Aishwarya Bhosale[2,3]*, Takeshi Matsui[4], and Carien M. Niessen[2,3,5]#, Chen Luxenburg[1]#, Matthias Rübsam[2,3,5]#

[1]Department of Cell and Developmental Biology, Faculty of Medical & Health Sciences, Tel-Aviv University, Tel-Aviv, Israel, [2]Department Cell Biology of the Skin, [3]Cologne Excellence Cluster for Stress Responses in Ageing-associated diseases (CECAD), University Hospital Cologne, University of Cologne, Cologne, Germany, [4]School of Bioscience and Biotechnology, Tokyo University of Technology, Tokyo, Japan, [5]Center for Molecular Medicine Cologne (CMMC), University Hospital Cologne, University of Cologne, Cologne, Germany.

Address correspondence to: Dr. Matthias Rübsam: ruebsam0@uni-koeln.de, Dr. Chen Luxenburg: lux@tauex.tau.ac.il, Dr. Carien M. Niessen: carien.niessen@uni-koeln.de

* These authors contributed equally to this work
# shared last authorship

Abstract

Cell shape and cell fate are tightly linked. However, how cortical cytoskeletal organization that controls cell shape connects to signaling and drives cell fate changes is still poorly understood. Here we used the skin epidermis as paradigm for spatiotemporally coordinated cell shape and fate changes. Upon induction of differentiation, epidermal stem cells stratify and increasingly flatten to form a functional barrier. Here, we identify spectrin, an actin-binding membrane cytoskeleton protein, as a major regulator of epidermal cell shape, signaling and differentiation to control the formation of a functional epithelial barrier. Loss of αII-spectrin (encoded by *Sptan1*) in the developing mouse epidermis inhibited suprabasal cell flattening, differentiation, and epidermal barrier function. Spectrin cortical localization required E-cadherin and actomyosin, while spectrin itself controls cortical actomyosin organization. In detail, using high resolution imaging and laser ablation revealed that spectrin was essential to form actin-based honeycomb-like cortical lattices that are essential to maintain cortical tension and structural integrity. We found that spectrin-dependent actomyosin organization controlled the activity and localization of the growth factor receptor EGFR, and the cation channel TRPV3, known to activate the enzyme transglutaminase essential for barrier function. Indeed, loss of spectrin, E-cadherin or actomyosin inhibition reduce TGM1 activity. Together, our results provide novel insights into how cortical organization and mechanics regulate cell shape and spatially activate signals necessary for differentiation and epithelial tissue function.

Introduction

Cells in our body exhibit a wide range of shapes, sizes, and functions, from giant, multinucleated, bone-degrading osteoclasts and contractile skeletal muscle cells to small, disc-shaped, a-nucleated red blood cells that carry oxygen (Luxenburg et al., 2007; Calderón et al., 2014; Elgsaeter et al., 1986). Defects in cell shape often correlate with tissue malfunction and manifestation of disease phenotypes. For instance, in many types of cancers, cells exhibit a wide range of abnormal cellular morphology (Lee et al., 2016; Kalluri and Weinberg, 2009). In muscular dystrophies, both cell shape and size are often abnormal (Delaporte et al., 1990; Emery, 2002). In sickle cell anemia, as the name suggests, cells lose their disc shape and unique mechanical properties (PAULING and ITANO, 1949). In common skin diseases such as psoriasis, atopic dermatitis as well as basal cell, and squamous cell carcinomas, keratinocytes exhibit abnormal cell shape, impaired differentiation and compromised epidermal barrier function (Koegel et al., 2009; Van Der Kammen et al., 2017). However, whether cell shape directly regulates cell differentiation and tissue function remains an open question.

At the body's surface, the interfollicular epidermis (hereafter, epidermis) is a stratified epithelium that functions as a barrier. The epidermis exhibits progressive cell shape changes. From cuboidal stem cells/progenitors that adhere to the underlying basement membrane, keratinocytes move to the spinous layer, increase in size and initiate flattening. When entering the first of the three granular layers (SG3-1 basal to apical), cells flatten extensively to take on the shape of kelvin's flattened tetrakaidecahedrons (Yokouchi et al., 2016), that is necessary to form and maintain the tight junctional (TJ) barrier in the SG2 (Kubo et al., 2009; Yoshida et al., 2013; Yokouchi et al., 2016; Rübsam et al., 2017), and ultimately terminal differentiation in the SG1. The latter process involves enucleation and transglutaminase (TGM)-mediated crosslinking of structural proteins and barrier lipids resulting in the formation of the stratum corneum barrier consisting of multiple layers of dead squames that physically separate the organism from the environment (Simpson et al., 2011a; Fuchs, 2007). Hence, the mammalian epidermis is an ideal model to address the relationship between cell position, shape and differentiation.

The actomyosin cytoskeleton represents a contractile subcellular machine made of actin fibers (F-actin), myosin II motor proteins, and dozens of additional actin-binding proteins that regulate the organization, dynamics, contractile state and thus the mechanical properties of the network (Pollard, 2016). Through its interaction with integrin-based cell-matrix junctions and cadherin-based cell-cell junctions (adherens junctions, AJs), this machinery is a major determinant of cell shape (Noordstra et al., 2023; Saraswathibhatla et al., 2023). Moreover, actomyosin activity modifies signaling cascades and the activity of transcription factors, thus links cell shape and cell differentiation/fate (Luxenburg and Zaidel-

Bar, 2019; Pollard, 2016; Zaidel-Bar et al., 2015). How the organization of these cortical actomyosin networks are spatially tuned to induce cell shape changes and how specific shape changes e.g. epidermal cell flattening are coupled to signaling is not fully understood.

In the epidermis, the amount of cortical F-actin increases with differentiation and cell flattening, a process regulated by E-cadherin (Rübsam et al., 2017). Moreover, epidermal cell shape is regulated by several distinct actin-binding proteins, including proteins that mediate actin-severing activity (i.e., cofilin, destrin, and WDR1) (Luxenburg et al., 2015); actin-sequestering protein thymosin β4(Padmanabhan et al., 2020), and the actin scaffolding protein anillin (Mahly et al., 2022). However, the loss of these proteins did not obviously impact epidermal differentiation. In contrast, the actin-related protein (Arp)2/3 complex, which enhances branched actin network assembly, is essential for epidermal differentiation and barrier formation but not tissue architecture (Zhou et al., 2013). It thus remains unclear whether a change in cell shape regulates epidermal differentiation.

Spectrins are unique actin-cross-linking cytoskeletal proteins that determine red blood cell shape and mechanical properties, and their loss of function results in severe anemia (Bodine et al., 1984; Gaetani et al., 2008; Pan et al., 2018). Spectrins are large and tensile spring-like proteins that can be detected predominantly at the cytoplasmic face of the plasma membrane, where they determine the mechanical properties of the cortical cytoskeleton, stabilize the juxtaposed plasma membrane, and organize submembrane compartments of plasma membrane proteins. Spectrins function as tetramers consisting of two α- and two β-spectrins. Vertebrates have two a-spectrin (αI and αII) and five β-spectrin (βI-βV). While αI-spectrin is detected only in erythrocytes, αII-spectrin (encoded by SPTAN1) is the only α-spectrin in non-erythrocyte cells that can interact with all five β-spectrin (Bennett and Healy, 2009; Bennett and Lorenzo, 2016; Teliska and Rasband, 2021). αII-spectrin loss-of-function leads to the early onset of West syndrome, an infantile epileptic syndrome that involves severe developmental delay and mental retardation (Saitsu et al., 2010). In mice, *Sptan1* knockout is embryonic lethal, and affected embryos exhibit neural tube, cardiac, and craniofacial defects and abnormal growth (Stankewich et al., 2011).

Previous studies in cultured keratinocytes have shown that spectrin levels increase in response to high calcium treatment, with its activity influencing early keratinocyte differentiation (Zhao et al., 2011, 2013; Wu et al., 2015). However, whether and how spectrin regulates the coordinated in vivo changes in keratinocyte cell shape and differentiation to form a functional in vivo skin barrier remains unknown.

In the present study, we investigated the roles of spectrin in epidermal development. We found that αII-spectrin levels increased during epidermal differentiation and that its cortical localization required

E-cadherin. At the cortex, spectrin governed actomyosin structural organization, activity, and mechanics. Moreover, E-cadherin-spectrin-mediated cortical tension regulated both cell shape and the activation of an EGFR/TRPV3 signaling pathway required for epidermal barrier formation. These observations provide novel insights into the complex links between cortical structural organization, mechanical properties, and biological regulation in a physiologically relevant mammalian system.

Results

Adherens junctions and αII-spectrin determine epidermal cell shape in the early granular layer

In the epidermis, transitions in cell fate and function coincide with changes in cell shape during differentiation. However, whether these changes in cell shape contribute to cell differentiation and fate is still largely unknown. Actomyosin contractility, through connection with cadherin-based adhesion receptors, is a key determinant of cell shape (Luxenburg and Zaidel-Bar, 2019; Niessen et al., 2024). We thus first asked whether epidermal cell shape depends on cell-cell contacts. To this end, we adapted a method (Matsui et al., 2021) based on exfoliative toxin to newborn mouse skin to separate the different layers and isolate individual cells from the spinous layer (SS)/SG3 layers and the SG2/SG1 layers. While SS/SG3 cells rounded up upon single-cell isolation, SG2/SG1 cells maintained their shape, indicating that cell shapes in the SG1/SG2 layers become independent of cell-cell contacts (Fig. 1a).

The contact-independent shape of the SG2/SG1 cells is reminiscent of red blood cells, in which spectrins function as major structural cortical elements to determine the shape of individual cells independent of cell-cell contacts (Leterrier and Pullarkat, 2022). Staining for non-erythrocytic spectrins in epidermal whole mounts and sections from newborn mice revealed αII-spectrin localization to cortical F-actin lattices throughout all layers of the epidermis, albeit with different intensity, indicating that spectrin is an integral part of the keratinocyte actomyosin cortex (Fig. 1b,c; Supplementary Fig. 1a). Quantification of αII-spectrin staining showed the highest cortical enrichment in the SG3 cells (Fig. 1d), whereas F-actin becomes increasingly more enriched when cells move upward, with the highest enrichment in SG1 cells (Fig. 1e), thus indicating that the cell shape changes that accompany differentiation are guided by changes in the ratio of actin and spectrin in the cortical actin lattices. Importantly, in the developing epidermis suprabasal αII-spectrin enrichmentment is first seen when suprabsal cell start to flatten at embryonic (E) day 15 (Supplementary Fig. 1b). Together, these data suggest that different ratios of spectrin/actin regulate the flattening of cells when they change position from spinous to the granular layer.

To determine whether αII-spectrin is required for cell flattening, we depleted αII-spectrin during epidermal development. The amniotic sacs of E9 wild-type mouse embryos were injected in utero with lentiviruses encoding *shSptan1-0595* or *shSptan1-9753* or *shScr* (control) together with a GFP-tagged histone 2B reporter (H2B-GFP) to identify transduced cells (Supplementary Fig. 1c-e)(Beronja et al., 2010). Depletion of αII-spectrin altered suprabasal but not basal cell shape, with cells being significantly less flat, showing that αII-spectrin drives suprabasal cell shape changes needed to achieve SG2/1 shapes (Fig. 1f,g).

To determine whether the F-actin-spectrin lattices also maintain the contact-independent cell shape of isolated SG1/SG2 cells, we disrupted actin filaments using latrunculin B in these cells. However, although F-actin was efficiently depolymerized, cell shape was not affected (Fig. 1h, i; Supplementary Fig. 1f, g), indicating that, unlike red blood cells, the contact-independent SG1/2 cell shapes are not maintained through a spectrin-actin membrane cytoskeleton (Leterrier and Pullarkat, 2022).

In simple epithelia, spectrins can be recruited to the cortex through E-cadherin-based AJ (Kizhatil et al., 2007; Machnicka et al., 2019; Pradhan et al., 2001; Nelson et al., 1990). We thus asked whether E-cadherin affects spectrin localization in the epidermis. To this end, we examined αII-spectrin localization in E-cadherin$^{epi-/-}$ mice (Tunggal et al., 2005). Loss of epidermal E-cadherin resulted in an almost complete inability to recruit spectrin to the cortex (Fig. 1j). However, E-cadherin maintained its proper localization in αII-spectrin-depleted epidermis (Fig. 1f). Consistently, depletion of E-cadherin in cultured keratinocytes led to mislocalization of αII-spectrin (Supplementary Fig. 1h), whereas depletion of αII-spectrin did not affect adherens junction (AJ) assembly during calcium switch experiments (Supplementary Fig. 1i). These findings collectively demonstrate that both in vivo and in vitro AJs function upstream in organizing the spectrin cytoskeletal network.

E-cadherin-based AJs regulate keratinocyte cell shape in vitro (Sahu et al., 2020b). To determine whether AJs regulate cell shape in vivo, we used the E-cadherin$^{epi-/-}$ mice to deplete suprabasal AJs and found a significant reduction in the flattening of SG cells in newborn mice (Fig. 1k,l; Supplementary Fig. 1h). Moreover, SG1/2 cells isolated from E-cadherin$^{epi-/-}$ were smaller than controls even if these cells still maintained their shape without cell-cell contacts (Fig. 1m; Supplementary Fig. 1i). Together, these results show that E-cadherin is essential to recruit αII-spectrin to the actin cortex, which is likely necessary to drive the transitions in cell shape that occur when epidermal cells differentiate and move through the different layers. In contrast, once cell shape is determined in the SG2 layer, cell shape becomes independent of both cell-cell-contact as well as of the spectrin-actin lattice.

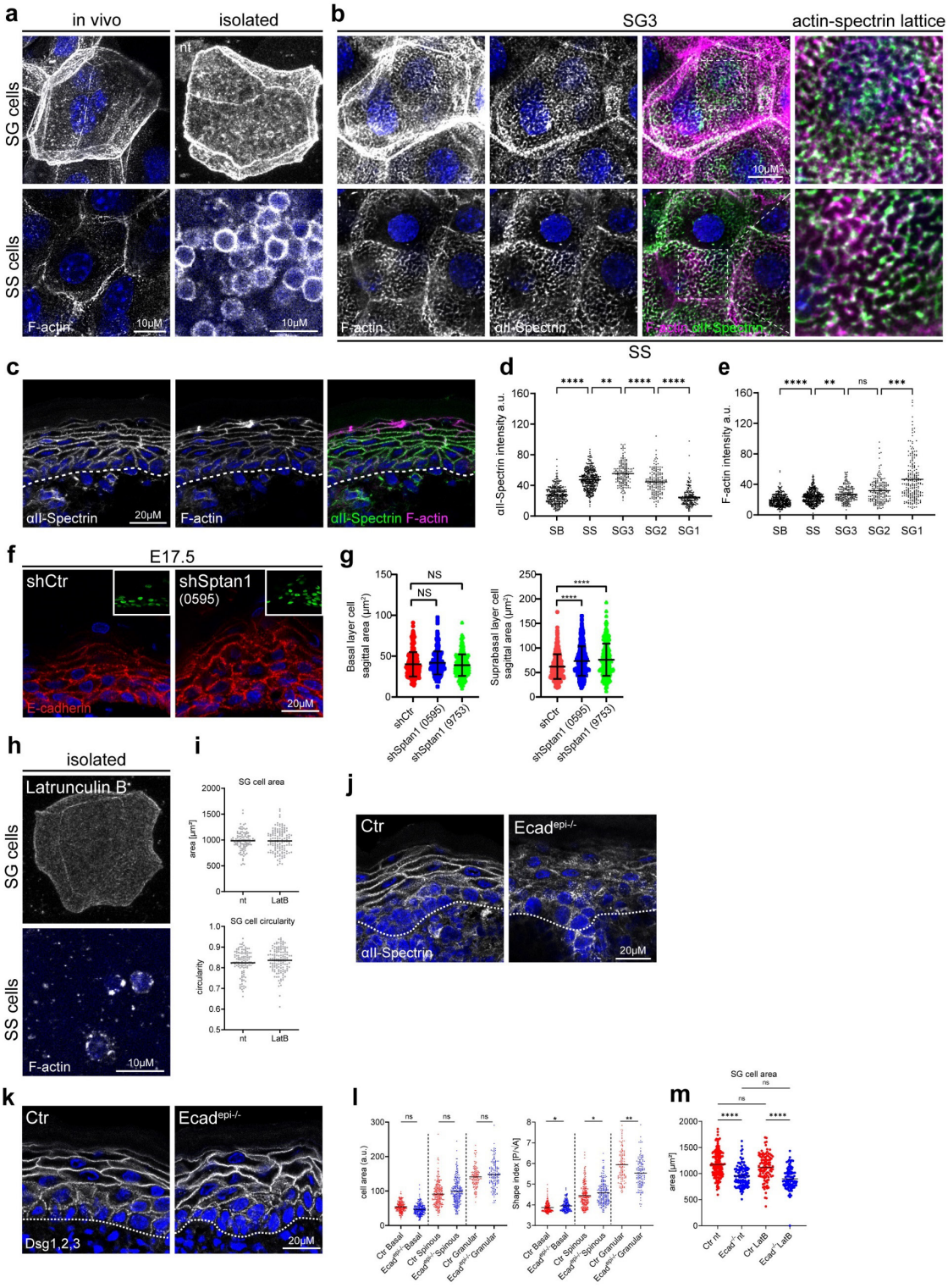

Figure 1 Adherens junctions and αII-spectrin determine epidermal cell shape in the early granular layer. **a** Newborn epidermal whole-mount immunofluorescence analysis for Phalloidin (F-actin) revealing cell shapes in the spinous (SS cells) and granular layer (SG cells) within tissue (in vivo). Right column: Phalloidin staining of single cells isolated from the spinous or granular layer showing deformation upon isolation only in spinous cells. **b** Newborn epidermal whole-mount immunofluorescence analysis for Phalloidin (F-actin) and αII-spectrin. Minimal max. projections of the spinous

(SS) and granular layer3 (SG3) are shown. **a,b** representative images of N≥3 biological replicates. **c** Immunofluorescence analysis for Phalloidin (F-actin) and αII-spectrin on newborn epidermis cryo sections. Representative image of n>3 biological replicates. **d,e** Quantification of cortical αII-Spectrin and F-actin intensity across the epidermal layers. Mean values (lines) of pooled cells (dots) from 3 mice. ****$P < 0.0001$, ***$P = 0.0001$, **$P < 0.007$; n≥157 cells with Kruskal–Wallis, Dunn's multiple comparison test. **f** Sagittal views of 10-µm dorsal skin sections from *shScr* (shCtr) and *shSptan1 0595* transduced E17.5 embryos immunolabeled for E-cadherin. Upper Insets show transduced cells (H2B−GFP+). **g** Quantification of cell cross-section area from data shown in **f**. Mean ± SD from ~200 individual cells from n=3 embryos per condition. Horizontal bars represent the basal layer cell cross-section area mean, and circles/squares/triangles represent individual cells. Not significant (P=0.1897 for basal *shSptan1 0595; P*=0.4090 for basal *shSptan1 9753*), ****P<0.0001 by unpaired t-test. Nuclei were stained with DAPI; dotted lines indicate the dermal-epidermal border. Scale bars = 20 µm. SBL, Suprabasal layer; NS, not significant. **h** Phalloidin staining of single cells isolated from the spinous or granular layer treated with Latrunculin B (0.1µM) showing deformation upon isolation only in spinous cells. **i** Quantification of the cell area and circularity of isolated SG cells (as shown in **h**) treated with or without Latrunculin B. Dots represent individual cells pooled from three mice. **j** αII-Spectrin staining on Ctr and E-cadherin deficient newborn epidermis sections showing impaired cortical recruitment of αII-Spectrin upon loss of E-cadherin. Representative images of n=3 biological replicates. **k** Immunofluorescence analysis for shape using combined staining for desmoglein1,2,3 (Dsg1,2,3) on Ctr and E-cadherin deficient newborn epidermis sections. **l** Quantification of cell area and shape/layer using stainings as shown in **k**. **$P < 0.005$, *$P < 0.03$; cells: n=420 (basal), n=445 (spinous), 277 (granular) with Kolmogorov-Smirnov per layer. **m** Quantification of the cell area of isolated SG cells from Ctr and E-cadherin deficient newborn epidermis and treated with Latrunculin B (0.1µM). Dots represent individual cells isolated from three mice. ****$P < 0.0001$; n≥98 cells with Kruskal–Wallis, Dunn's multiple comparison test. All images: Nuclei were stained with DAPI (blue).

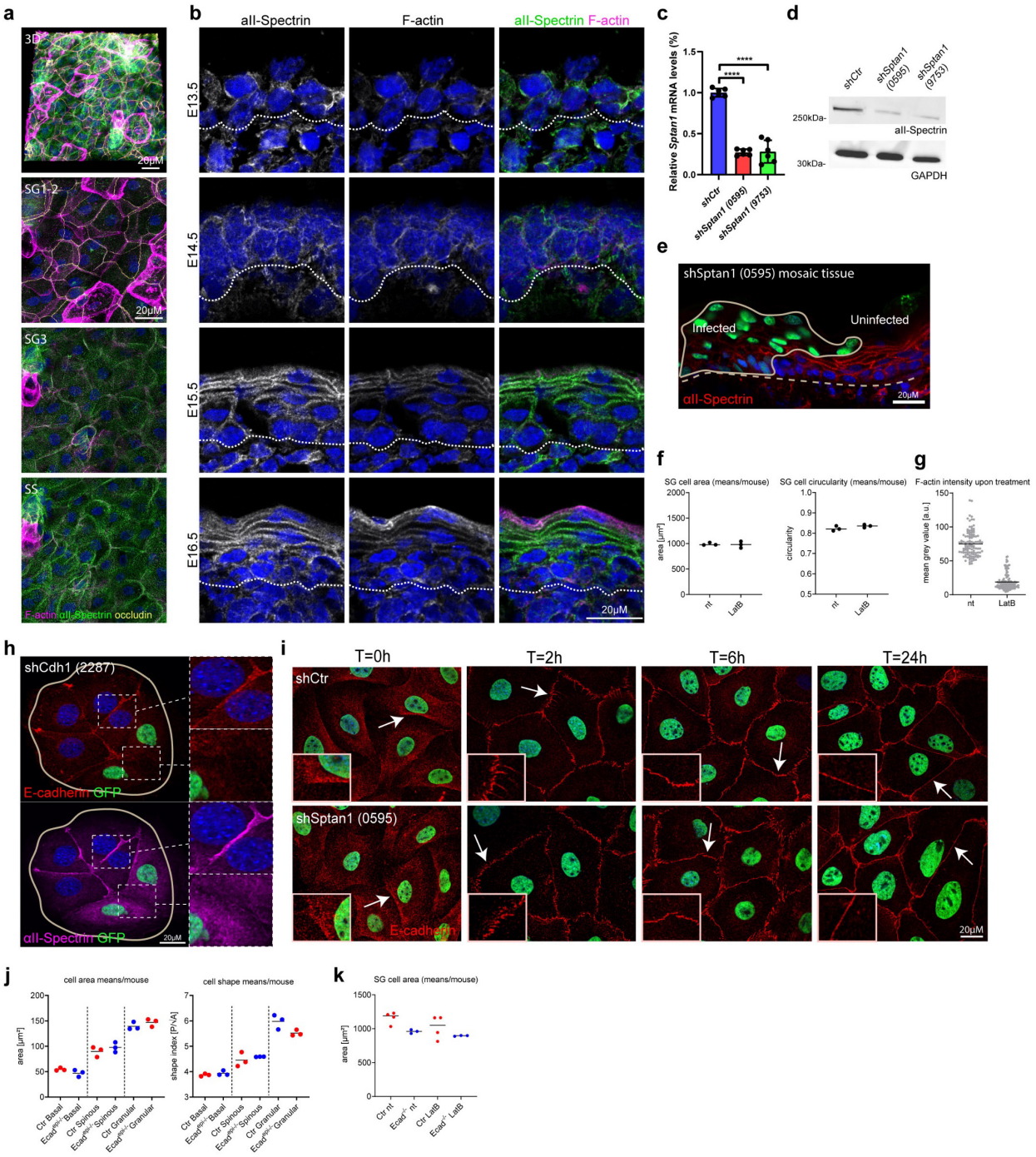

Supplementary Figure 1 AJs and αII-spectrin determine epidermal cell shape in the early granular layer. **a** Newborn epidermal whole-mount immunofluorescence analysis for Phalloidin (F-actin), αII-spectrin and tight junction marker occludin marking the SG2 layer. Overview of protein distribution across layer corresponding to Fig. 1b. Minimal max. projections of the epidermal layers and a full projection (3D) are shown. **b** Immunofluorescence analysis for Phalloidin (F-actin) and αII-spectrin on newborn epidermis cryo sections of embryonic timepoints as indicated. Dashed line marks the epidermal-dermal boarder. **a,b** representative images of N≥3 biological replicates. **c** Quantitative qPCR analysis of *Sptan1* mRNA in primary mouse keratinocytes transduced with scrambled (shCtr) shRNA or one of two *Sptan1* -specific shRNAs (0595 and 9753). Mean ± SD of six preparations. ****P <0.0001 by unpaired t-test. **d** Western blot analysis of primary mouse keratinocytes transduced with *Scr*, *Sptan1 0595*, or *Sptan1 9753* shRNAs. **e** sagittal views of 10-µm dorsal skin mosaic tissue sections from *shSptan1 0595* transduced E17.5 embryos immunolabeled for

αII-spectrin. Circular line indicates areas of infected cells. Nuclei were stained with DAPI; dashed lines indicate the dermal-epidermal border. **f** Quantification of the cell area and circularity of isolated SG cells treated with or without Latrunculin-B treatment (corresponding to Fig. 1i). Dots represent mean values per mouse. Not significant; n = 3 biological replicates with Mann–Whitney test. **g** Quantification of F-actin intensity (Phalloidin) of isolated SG cells (as shown in **Fig. 1h**) treated with or without Latrunculin B. Dots represent individual cells pooled from three mice. **h** Immunofluorescence analysis for the recruitment of E-cadherin and αII-spectrin to intercellular contacts in *scrambled* (shCtr) and *shCdh1 2287* transduced primary keratinocytes (GFP positive nuclei). Representative images of n=3 biological replicates each. **i** Immunofluorescence analysis for E-cadherin (red) based early intercellular contacts in *shScr* (shCtr) and *shSptan1 0595* transduced primary keratinocytes (6h Ca2+). Representative images of n=3 biological replicates each. **j** Quantification of cell area and shape/layer (corresponding to Fig. 1k,l). Dots represent mean values per mouse. **k** Quantification of the cell area of isolated SG cells from Ctr and E-cadherin deficient newborn epidermis treated with or without Latrunculin B (0.1µM) (corresponding to **Fig. 1m**). Dots represent mean values per mouse.

Cortical F-actin and spectrin organization are mutually dependent in vivo

Two of the major spectrin binding partners, the adaptor protein ankyrin and F-actin (Bennett and Healy, 2009; Bennett and Lorenzo, 2016), also interact with E-cadherin directly or indirectly (Kong et al., 2023) and may thus be downstream of E-cadherin to recruit spectrin to the cortex. Staining of E17.5 embryos for ankyrin G (encoded by *Ank3*), the only ankyrin expressed in the epidermis (Sennett et al., 2015), revealed cortically enriched ankyrin G in the granular layer (Fig. 2c, control). However, depletion of *Ank3* in E17.5 embryos did not alter either spectrin localization or levels (Fig. 2a, b; Supplementary Fig. 2a-c). In line, we also detected no changes in F-actin and cell shape in ankyrin G-depleted epidermis (Supplementary Fig. 2d-g). In contrast, depletion of αII-spectrin decreased ankyrin cortical levels (Fig. 2c-e). Thus, spectrin cortical recruitment is independent of ankyrin but regulates robust ankyrin recruitment to the cortex.

To determine whether F-actin regulates spectrin localization and levels, E17.5 embryos were treated with low levels of Latrunculin B (2.5µM) to reduce F-actin levels but not interfere with cell adhesion itself, as indicated by unaltered E-cadherin localization at cell borders (Supplementary Fig. 2h). Latrunculin B treatment reduced cortical αII-spectrin levels in all layers of the epidermis (Fig. 2f, g). Because the cortex of keratinocytes in the developing epidermis is highly enriched for Myosin II (Dor-On et al., 2017; Sumigray et al., 2012), we also treated embryos with the rho-associated protein kinase (Rock) inhibitor, Y27632, to reduce myosin II contractile activity. Similar to latrunculin treatment, a decrease in cortical αII-spectrin levels was observed (Fig. 2f,g), suggesting that αII-spectrin recruitment depends on actomyosin activity. Next, we asked whether F-actin organization and levels depend on αII-spectrin. Embryonic KD of αII-spectrin reduced cortical F-actin levels specifically in the suprabasal layers of E17.5 embryos, in line with αII-spectrin enrichment in suprabasal layers (Fig. 2h,i). These results demonstrate that F-actin and spectrin cortical localization and organization are interdependent. On the other hand, ankyrin G is dispensable for spectrin localization and regulation of cell shape in the epidermis.

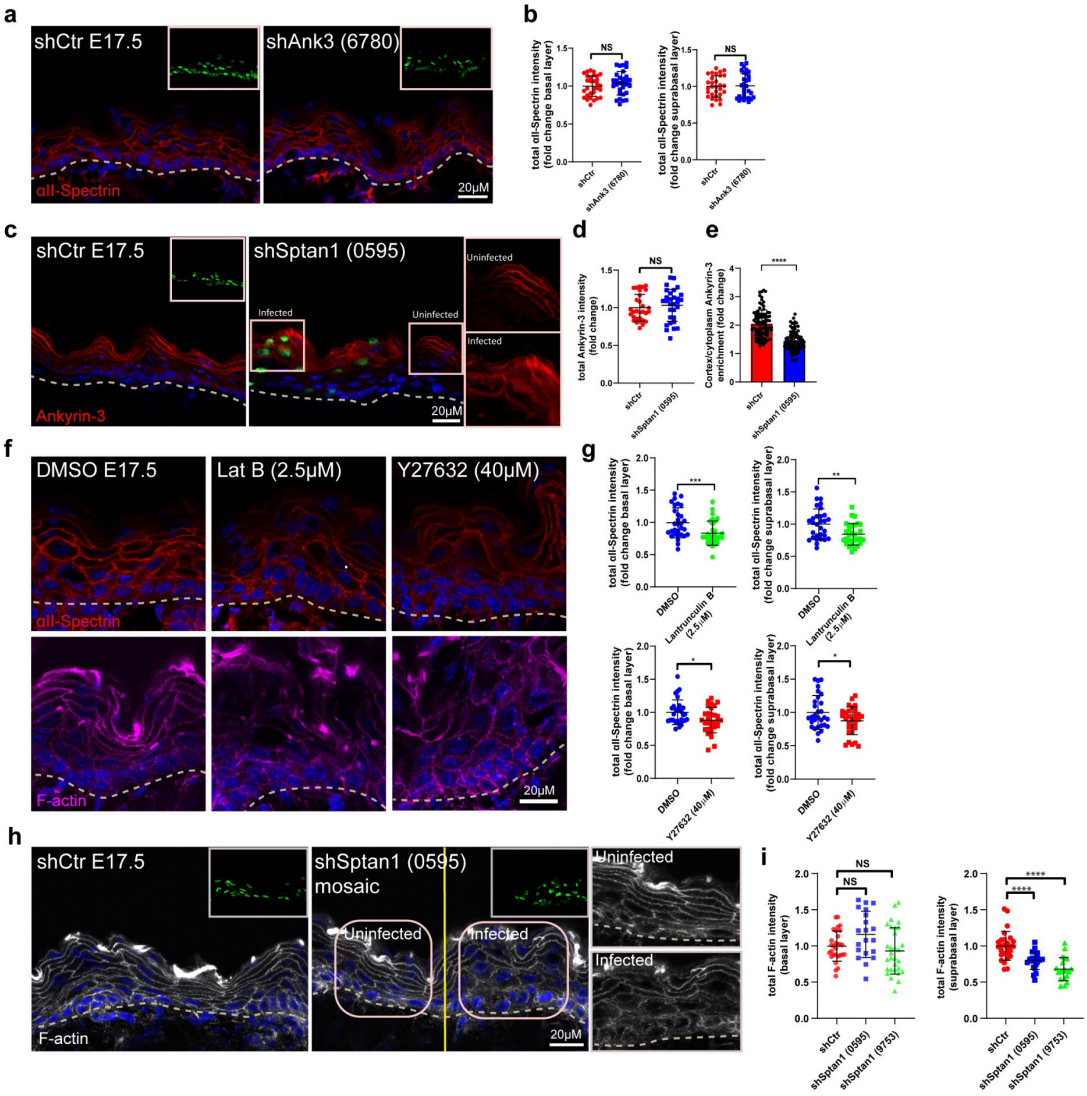

Figure 2 Cortical F-actin and spectrin organization are mutually dependent in vivo. **a** Sagittal views of 10-µm dorsal skin sections from *shScr* (shCtr) and *shAnk3 6780* transduced E17.5 embryos immunolabeled for αII-spectrin (Red). Insets show the transduced cells (H2B−GFP+). **b** Quantification of basal (left) and suprabasal (right) layer αII-spectrin intensity from data shown in **a**. Data are the mean ± SD of 30 ROI (Region of interest) from n=3 embryos per condition. Horizontal bars represent the mean normalized intensity, and circles/squares represent individual microscopy fields. NS: *P*=0.3199 (basal), NS: *P*=0.8256 by unpaired t-test. **c** Sagittal views of 10-µm dorsal skin sections from *shScr* (shCtr) and mosaic *shSptan1 0595* transduced E17.5 embryos immunolabeled for Ankyrin-3. Upper insets show the transduced cells (H2B−GFP+). Insets (right) show the magnification of boxed areas. **d** Quantification of Ankyrin-3 intensity from data shown in **c**. Data are the mean ± SD of 30 ROI (Region of interest) from n=3 embryos per condition. Horizontal bars represent the mean normalized intensity, and circles/squares represent individual microscopy fields. NS: *P*=0.512 by unpaired t-test. **e** Quantification of Ankyrin-3 cortical enrichment from the data shown in **c**. Data are the mean ± SD from 90 individual cells from n=3 embryos per condition. Horizontal bars represent the Ankyrin-3 cortex/cytoplasm intensity ration mean and circles represent individual cells. ****P <0.0001 by unpaired t-test. **f** Sagittal views of 10-µm dorsal skin sections from E17.5 wild-type embryos treated with DMSO, latrunculin B, and Y27632 immunolabeled for αII-spectrin and F-Actin. **g** Quantification of basal (left graphs) and suprabasal (right graphs) layer αII-spectrin intensity from data shown in **f**. Data are the mean ± SD of 30 ROI (Region of interest) from n=3 embryos per condition. Horizontal bars represent the mean normalized intensity, and circles/squares represent individual microscopy fields. ***P=0.005 (basal, latrunculin B), **P=0.0044 (suprabasal, latrunculin B), *P=0.0165 (basal, Y27632), *P=0.0394 (suprabasal, Y27632) by unpaired t-test. **h** Sagittal views of 10-µm dorsal skin sections

from *shScr* (shCtr) and mosaic *shSptan1 0595* transduced E17.5 embryos immunolabeled for F-actin (gray). Upper insets show the transduced cells (H2B−GFP+). Insets (right) show the magnification of boxed areas. **i** Quantification of basal (left) and suprabasal (right) layer F-actin intensity from data shown in **h**. Data are the mean ± SD of 30 ROI (Region of interest) from n=3 embryos per condition. Horizontal bars represent the mean normalized intensity, and circles/squares/triangles represent individual microscopy fields. NS: *P*=0.0553 (*shSptan1 0595, basal), P*=0.2818 (*shSptan1 9753, basal), ****P*=0.0004 (*shSptan1 0595, suprabasal), ****P*=0.0006 (*shSptan1 9753, suprabasal)* by unpaired t-test. Nuclei were stained with DAPI, dotted lines indicate the dermal-epidermal border. NS, not significant.

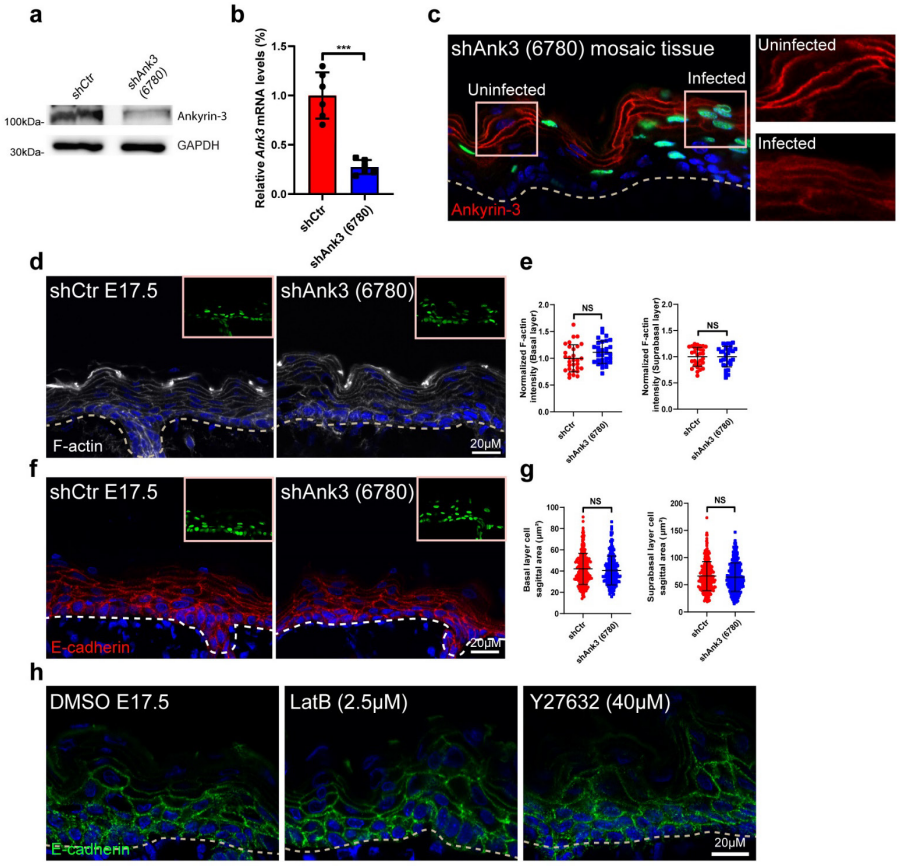

Supplementary Figure 2 Cortical F-actin and spectrin levels are mutually dependent in vivo. **a** Western blot analysis of primary mouse keratinocytes transduced with scrambled (shCtr) and *Ank3 6780* shRNAs. Blots were probed for Ankyrin-3 and GAPDH. **b** qPCR analysis of *Ank3* mRNA in primary mouse keratinocytes transduced with scrambled (shCtr) shRNA or *Ank3* specific shRNAs (6780). Data are the mean ± SD of six preparations. ***P=0.0004 by unpaired t-test. **c** sagittal views of 10-µm dorsal skin mosaic tissue sections from *shAnk3 6780* transduced E17.5 embryos immunolabeled for Ankyrin-3. Insets (right) show the magnification of uninfected and infected boxed areas. **d** Sagittal views of 10-µm dorsal skin sections from *shScr* (shCtr) and *shAnk3 6780* transduced E17.5 embryos immunolabeled for F-actin (grey). Insets show transduced cells (H2B−GFP+). **e** Quantification of basal (left) and suprabasal (right) layer F-actin intensity from data shown in **d**. Data are the mean ± SD of 30 ROI (Region of interest) from n=3 embryos per condition. Horizontal bars represent the mean normalized intensity, and circles/squares represent individual microscopy fields. NS: P=0.0692 (basal), NS: P=0.9506 (suprabasal) by unpaired t-test. **f** Sagittal views of 10-µm dorsal skin sections from *shScr* (shCtr) and *shAnk3 6780* transduced E17.5 embryos immunolabeled for E-cadherin. Insets show transduced cells (H2B−GFP+). **g** Quantification of basal (left) and suprabasal (right) layer cell cross-section area from data shown in **g**. Data are the mean ± SD from~ 200 individual cells from n=3 embryos per condition. Horizontal bars represent the cell cross-section area mean, and circles/squares represent individual cells. NS: P=0.2389 (basal), NS: P=0.3531 (suprabasal) by unpaired t-test. **h** Sagittal views of 10-µm dorsal skin sections from E17.5 wild-type embryos treated with DMSO, latrunculin, and Y27632 immunolabeled for E-cadherin. Nuclei were stained with DAPI; dotted lines indicate the dermal-epidermal border. NS, not significant.

Spectrin determines junctional actomyosin network structure and stability

To better understand the organization and mechanics of the αII-spectrin-F-actin lattice, we isolated primary keratinocytes and switched cells from low (50 µM) to high Ca^{2+} (1.8 mM) to induce cadherin-dependent cell-cell adhesion and subsequent stratification and differentiation. Upon initial E-cadherin engagement (6h Ca^{2+}) only F-actin but not spectrin is recruited to early AJ, so called AJ zippers (Fig. 3a,b), to form peri-junctional rings (Vasioukhin et al., 2000) (Fig. 3a,b). Consistently, αII-spectrin knockdown did not alter AJ formation. initial E-cadherin engagement (6h Ca^{2+})(Supplementary Fig. 3a).

Long term differentiation and stratification of keratinocytes into a multilayer (48h Ca^{2+}) upregulated spectrin protein levels (Supplementary Fig. 3a,b, 2.28 fold compared to 6h Ca^{2+}), in agreement with the *in vivo* increase in cortical levels of spectrin in suprabasal layers (Fig. 1c,d). Importantly, spectrin now co-localized with F-actin to form micro-honeycomb like cortical lattices that through AJs link to the plasma-membrane, a configuration that is highly similar to its organization in differentiated, suprabasal layers of the epidermis (Fig. 3a,b). Spectrin was also localized to the F-actin cortical ring that supports barrier-forming TJs in the most upper apical cell layer, albeit to a much lesser extent than F-actin (Fig. 3a,b)(Rübsam et al., 2017). In contrast, very little αII-spectrin was recruited to the diffuse F-actin cortex underneath the apical membrane that is free of cell-cell contact (Fig. 3a,b), in agreement with our observation that E-cadherin is essential to recruit αII-spectrin to the cortex. Similar to *in vivo*, Latrunculin B treatment disturbed cortical αII-spectrin recruitment in cultured keratinocytes (Supplementary Fig. 3c). Thus, in primary keratinocytes AJs reorganize the F-actin cortex upon differentiation and stratification that then recruit αII-spectrin to form the micro-honeycomb like lattices, similar to what is observed in vivo.

We next asked whether spectrin is required for the organization of junctional F-actin into these honey-comb lattices. Strikingly, αII-spectrin KD resulted in a complete loss of the honeycomb structure with F-actin now organized into linear fibers (Fig. 3c; Supplementary Fig. 3h), that resemble F-actin stress fibers, thus suggesting a change in actomyosin contractile forces. In contrast, αII-spectrin KD did not affect the formation of the apical TJ-associated F-actin cortical ring of the most apical cells, even though F-actin levels were reduced at these rings (Supplementary Fig. 3d-g).

To directly ask whether myosin activity is necessary to organize suprabasal spectrin-F-actin lattices, we lowered myosin contractile activity with a low dose of blebbistatin (5µM). This treatment disassembled the honeycomb spectrin-F-actin structure in control keratinocytes into a diffuse F-actin organization, showing that next to spectrin, myosin activity is also necessary for the organization into honeycomb cortical networks. Moreover, Blebbistatin treatment also resolved the linear F-actin fibers

upon αII-spectrin KD, showing that these are fibers are indeed under tension (Fig. 3d; Supplementary Fig. 3h).

To directly assess whether αII-spectrin controls the mechanical properties of the suprabasal actomyosin cortex we performed linear laser ablation experiments in keratinocytes incubated with SiR-actin to label F-actin, and measured the strain-dependent recoil. Ablation of the cortex in control keratinocytes resulted in elliptical openings increasing in size over time (Supplementary Fig. 3i), indicative of visco-elastic behavior of the cortex as previously shown (Saha et al., 2016; Thi Kim Vuong-Brender et al., 2017). Moreover, curved intercellular borders straightened upon ablation, suggesting that tension generated by the actomyosin-spectrin honeycomb networks is transferred to AJs to regulate cell shape (Supplementary Fig. 3j). Importantly, depleting αII-spectrin resulted in a fast and highly irregular recoil, with ultimate 2-fold larger, highly irregularly shaped openings, thus indicating that the reorganization into F-actin fibers upon loss of spectrin decreased cortical coherence (Fig. 3e,f). As E-cadherin is essential for cortical spectrin-F-actin organization, we predicted that E-cadherin also regulates the visco-elastic properties of the network. Similar to αII-spectrin KD, upon loss of E-cadherin recoil was highly irregular with 3.86-fold larger opening than Ctr (Fig. 3g,h), thus indicating that E-cadherin controls the mechanics of suprabasal cells through spectrin. Interestingly, blebbistatin treatment of αII-spectrin KD cells rescued the increased recoil of the cortex upon ablation, suggesting that spectrin-dependent honeycomb organization is necessary to dissipate tension across the network to prevent damage (Fig. 3i,j). Taken together, these data suggest a model in which E-cadherin through indirect spectrin recruitment determines the stability of cortical actomyosin lattices under tension.

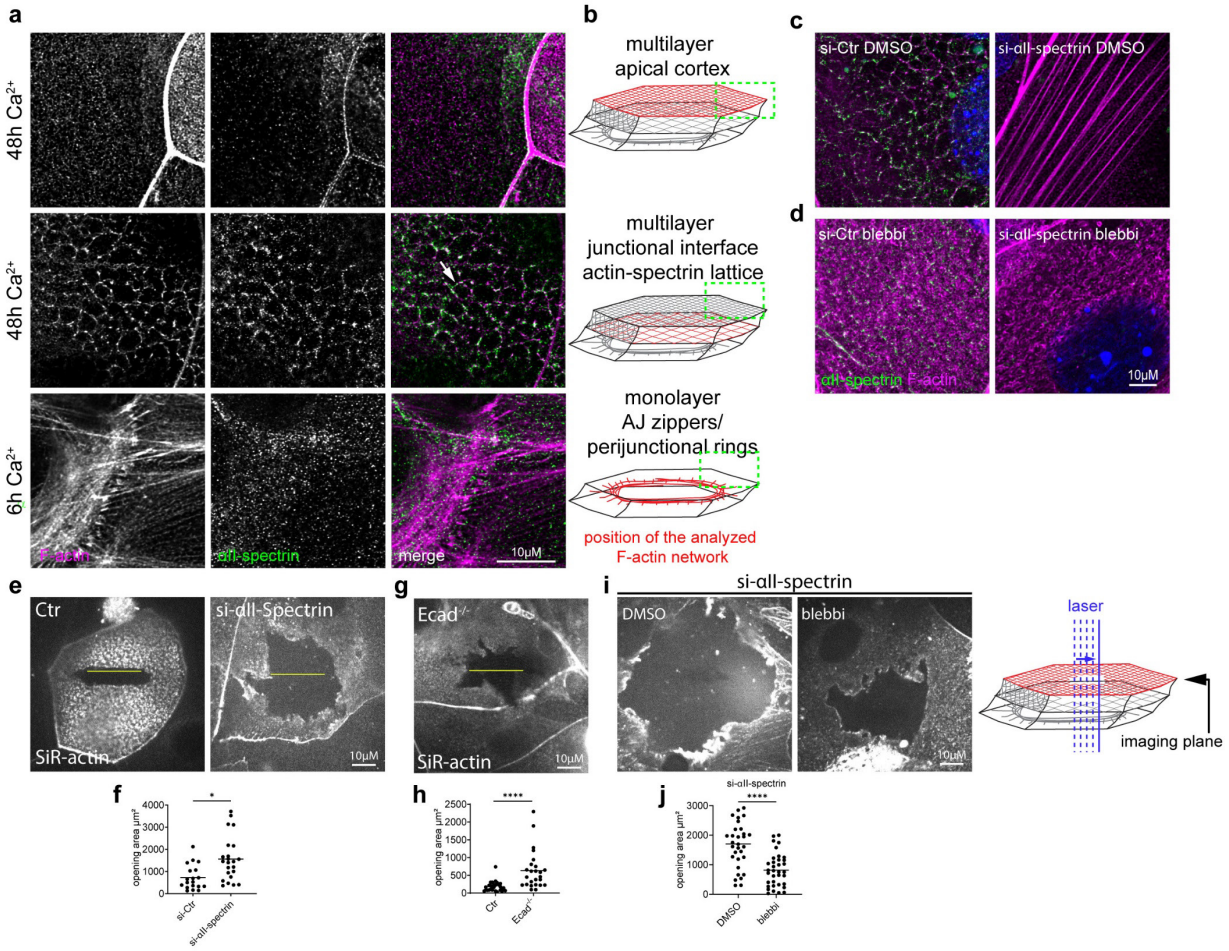

Figure 3 Spectrin determines junctional actomyosin network structure and stability. **a** Immunofluorescence analysis for αII-Spectrin and F-actin after 6h or 48h in high Ca^{2+} at cell-cell interfaces (arrow: actin-spectrin lattice) and apical surface. Representative images of n≥3 biological replicates each. **b** Schematic representation of the image position in the mono or multilayered keratinocytes. **c,d** Immunofluorescence analysis for αII-spectrin and F-actin (48h high Ca^{2+}) upon αII-spectrin knockdown and treatment with either DMSO (**c**) or low dose blebbistatin (5µM)(**d**). Representative images of n=3 biological replicates each. **e** Laser ablation: Live imaging of SiR-actin (F-actin) labeled Ctrand αII-spectrin knockdown keratinocytes after 48h high Ca^{2+}. Cells are depicted 10 seconds after a linear laser cut (yellow line). The opening (damage) in the F-actin cortex upon linear laser ablation is seen as black area around the yellow line. **f** Quantification of opening areas in the apical F-actin cortex upon linear laser ablation as shown in **e**. Lines represent means, dots represent single openings/cells pooled from n=3 independent experiments/biological replicates. **P*=0.0215 with Kolmogorov-Smirnov. **g** Laser ablation (as described for **e**) of E-cadherin$^{-/-}$ keratinocytes after 48h high Ca^{2+}. **h** Quantification of opening areas in the apical F-actin cortex upon linear laser ablation as shown in **g**. Lines represent means, dots represent single openings/cells pooled from n=3 independent experiments/biological replicates. ****P<0.0001 with Kolmogorov-Smirnov. **i** Laser ablation (as described for **e**) of αII-spectrin knockdown keratinocytes treated with DMSO or low dose blebbistatin (5µM) 1h prior to ablation. **j** Quantification of opening areas in the apical F-actin cortex upon linear laser ablation as shown in **i**. Lines represent means, dots represent single openings/cells pooled from n=3 independent experiments/biological replicates. *****P*<0.0001 with Kolmogorov-Smirnov.

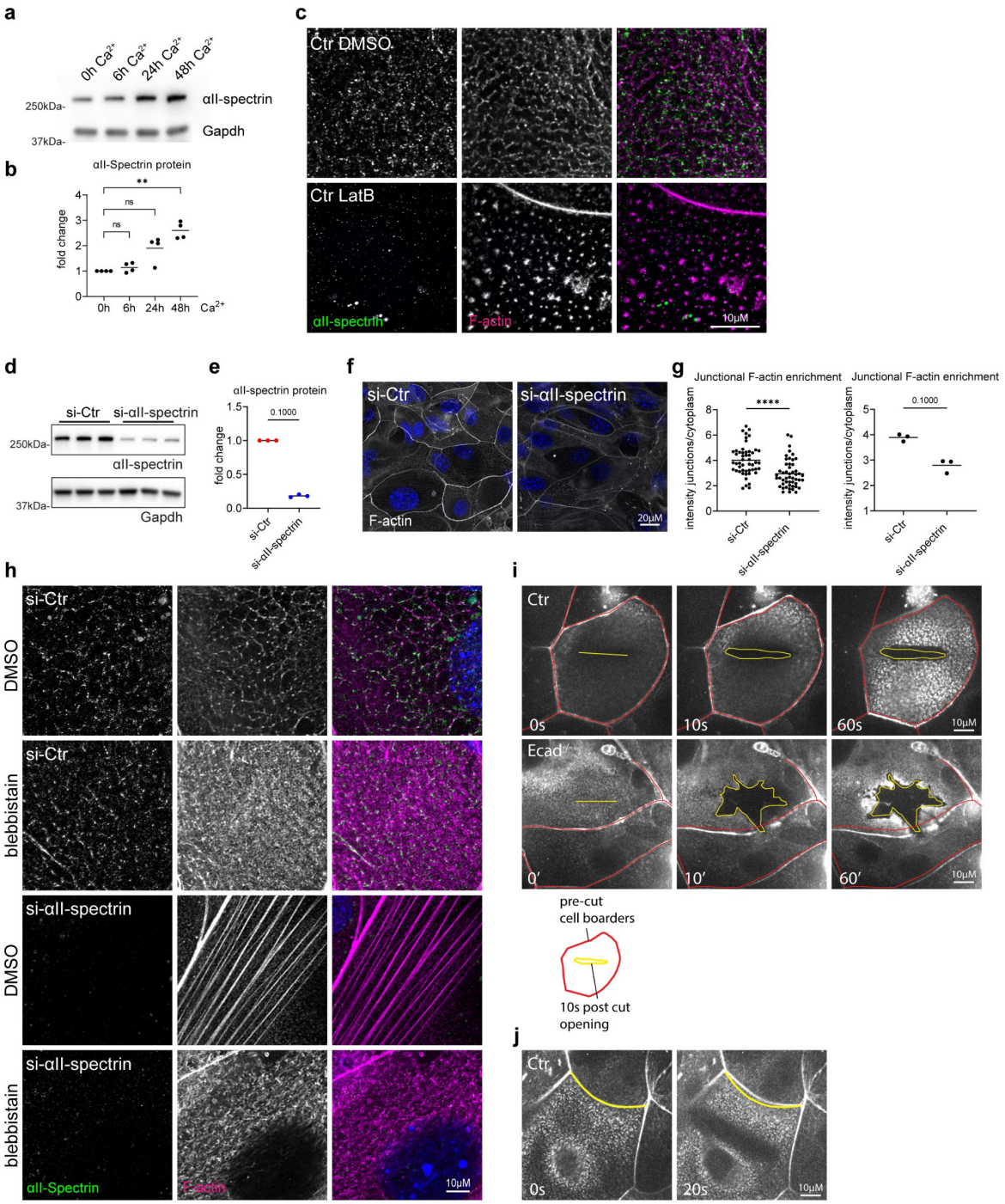

Supplementary Figure 3 Spectrin determines junctional actomyosin network structure and stability. **a** Western blot analysis for αII-spectrin protein levels after Ca^{2+} switch for the timepoint indicated. **b** Western blot quantification for αII-spectrin as shown in **a**, normalized to GAPDH and to 0h Ca^{2+} timepoint. Dots represent biological replicates from n=4 independent primary keratinocyte isolates. ***P*=0.003 with Kruskal–Wallis, Dunn's multiple comparison test. **c** Immunofluorescence analysis for αII-spectrin and F-actin after 48h in high Ca^{2+} at cell-cell interfaces with and without Latrunculin B treatment (1h, 0.1μM). **d** Western blot analysis for αII-spectrin protein levels upon siRNA (siPools) mediated knockdown 96h post transfection (72h Ca^{2+}). **e** Western blot quantification for αII-spectrin as shown in **d**, normalized to GAPDH. Dots represent biological replicates, n=3 with Mann-Whitney. Representative example of n=6 independent primary keratinocyte isolates. **f** Immunofluorescence analysis of F-actin organization at apical junction

rings after 48h in high Ca^{2+} and siRNA mediated knockdown of αII-spectrin. **g** Left graph: Quantification of F-actin intensity at apical junction rings (mean grey value, junctions/cytoplasm) as shown in **f**. Dots represent pooled values of single cells from n=3 biological replicates. ****$P<0.0001$ with Kolmogorov-Smirnov. Right graph: Mean values from n=3 biological replicates tested with Mann-Whitney. **h** Immunofluorescence analysis for αII-spectrin and F-actin (48h high Ca^{2+}) upon αII-spectrin knockdown and treatment with either DMSO or low dose blebbistatin (5µM). Representative images of n=3 biological replicates each. Single channel grey scale and merged channels corresponding to **Fig. 3c,d**. **i** Laser ablation: Live imaging of SiR-actin (F-actin) labeled Ctr keratinocytes after 48h high Ca^{2+} showing expansion of cell-cell boarders (red lines) and expansion of the immediate opening (yellow shape) upon laser cut (yellow line). Cells are depicted 10 and 60 seconds after a linear laser cut (yellow line). **j** Laser ablation as described for **i** showing straightening of curved cell-cell boarders (yellow line) after linear ablation of the distal cortex.

αII-spectrin activity enhances epidermal barrier formation

Our results thus far demonstrate that αII-spectrin is essential for suprabasal cell flattening that is a hallmark of epidermal differentiation (Simpson et al., 2011a; Luxenburg and Zaidel-Bar, 2019) To ask whether this change in shape induced by depletion of αII-spectrin directly links to changes in epidermal differentiation, weassessed the expression of the epidermal cell markers keratin 14 (K14, basal layer), K10 (suprabasal layers), and loricrin (granular layer). The back skin epidermis from E17.5 control embryos showed uniform K14 staining in a single basal layer. In contrast, in the epidermis from *Sptan1* KD embryos $K14^+$ cells were also detected suprabasally (Fig. 4a). Suprabasal cells were still also positive for the differentiation marker K10 (Fig. 4a), indicating that spectrin is essential for robust initiation of differentiation when basal cells move suprabasally. Finally, in control back skin, $loricrin^+$ granules filled the entire cytoplasm of granular layer cells. In contrast, in the back skin of *Sptan1* KD embryos, loricrin was detected predominantly at the cell periphery (Fig. 4a), suggesting that SG differentiation was abnormal. These differentiation defects were also recapitulated in embryos transduced with a second *Sptan1 shRNA* (Sptan1-9753; Supplementary Fig. 4a).

Two of the hallmarks of the SG are the ion- and size-selective barrier forming TJs that also depend on and link to actomyosin (Rübsam et al., 2017; Sumigray et al., 2012) and the Ca^{2+}-dependent activation of the cross-linker enzymes transglutaminases (TGM) (Eckert et al., 2005). These two processes are crucial in the epidermal inside-out and outside-in barrier formation, respectively (Simpson et al., 2011). Therefore, we asked whether these processes are altered without αII-spectrin. To accurately measure TJ activity, we utilized primary keratinocytes, which form functional TJs as measured by transepithelial electrical resistance (TEER) upon the Ca^{2+} switch. Knocking down αII-spectrin in isolated primary keratinocytes revealed major defects in TEER formation, indicating TJ dysfunction (Fig. 4b).

Next, we conducted a TGM1 activity assay based on crosslinking of fluorophore-coupled substrate peptides (Sugimura et al., 2008). In the back skin from the control E17.5 embryos, TGM substrate was highly enriched at the cell cortex, while in *Sptan1* KD E17.5 embryos, we observed a ~30% decrease in cortical enrichment and an overall decrease of 13% in TGM substrate fluorescence intensity (Fig. 4c-e). In line with the notion that E-cadherin is essential to recruit spectrin to the cortex of the developing epidermis, E-$cadherin^{epi-/-}$ epidermis also showed decreased TGM activity (Fig. 4f,g; Supplementary Fig. 4b).

To determine whether these defects in TJs and TGM activity affect the establishment of a functional epidermal barrier, we treated E17.5 control and *Sptan1* KD embryos with toluidine blue (Hardman et al., 1998). As expected, control embryos excluded the dye and were not stained, indicating

an intact barrier. In contrast, employing two different shRNA against Sptan1 showed staining in the head and ventral parts of the embryo, demonstrating that αII-spectrin activity is essential for the formation of a functional epidermal barrier (Fig. 4h; Supplementary Fig. 5c).

***Sptan1* depletion does not alter YAP localization.**

Next, we addressed how αII-spectrin activity enhances epidermal barrier formation. In both *Drosophila* and cultured human simple epithelial cells, spectrin controls YAP localization and hippo signaling (Deng et al., 2015; Fletcher et al., 2015). Moreover, in the developing mouse epidermis, an increase in YAP nuclear localization, indicative of active YAP, impairs epidermal barrier formation (Zhou et al., 2013). We thus asked whether YAP nuclear localization was changed upon loss of αII-spectrin. Immunostaining for YAP in E17.5 control and *Sptan1* detected comparable numbers of YAP+ nuclei in both basal and suprabasal layers in the control and *Sptan1*-depleted epidermis (38.6% ±0.9% vs. 40.4%±1.6% and 22.6% ±3% vs 23.1% ±3.9%, respectively) (Supplementary Fig. 4d,e), thus suggesting that loss of αII-spectrin did not alter YAP activity.

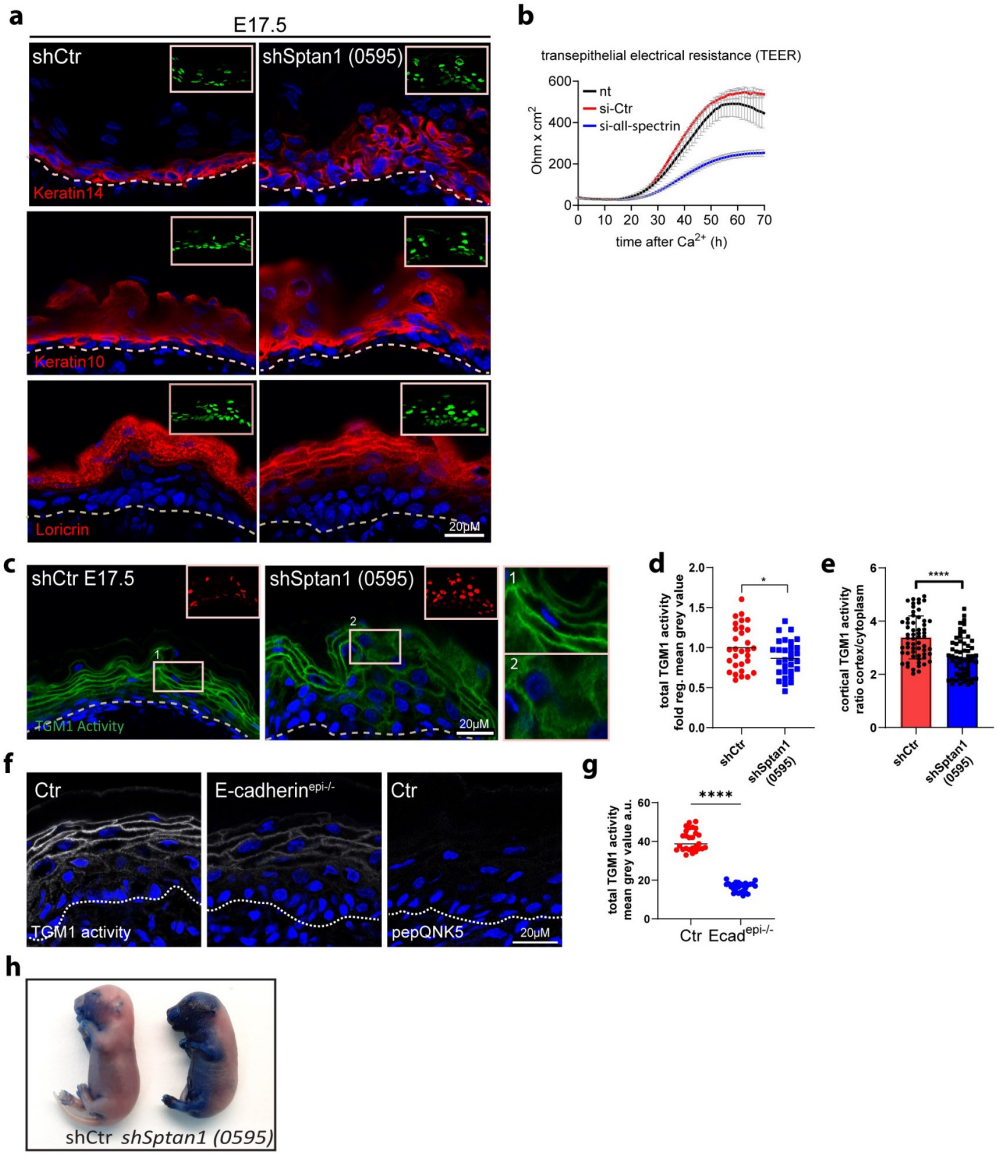

Figure 4 αII-spectrin regulates epidermal differentiation and barrier function. **a** Sagittal views of 10-µm sections of dorsal skin from *shScr* (*shCtr*) and *shSptan1 0595* transduced E17.5 embryos immunolabeled for the basal layer marker K14, the differentiation marker K10 and the granular layer marker loricrin. Insets show the transduced cells (H2B−GFP+). **b** Transepithelial resistance (TER) measurements in Ctr and αII-spectrin knockdown keratinocytes after switching to high Ca^{2+}. Line represent means over time of 3 biological replicates each. Representative experiment of n > 10 biological replicates. **c** Sagittal views of 10-µm sections of dorsal skin from *shScr* (*shCtr*), and *shSptan1 0595* transduced E17.5 embryos. Sections were processed for Transglutaminase1 (TGM1) activity assay. Upper Insets show the transduced cells (H2B−RFP+). Insets (right) show the magnification of the boxed areas. **d** Quantification of TGM1 intensity from data shown in **c**. Data are the mean ± SD of 30 ROI (Region of interest) from n=3 embryos per condition. Horizontal bars represent the mean normalized intensity, and circles/squares represent individual microscopy fields. **P*=0.0471 by unpaired t-test. **e** Quantification of TGM1 activity cortical enrichment from the data shown in **c**. Data are the mean ± SD from 60 individual cells from n=3 embryos per condition. Horizontal bars represent the TGM1 activity cortex/cytoplasm intensity ratio mean, and circles/squares represent individual cells. *****P*<0.0001 by unpaired t-test. **f** Sagittal views of 10-µm sections of dorsal skin from Ctr and E-cadherin$^{epi-/-}$ newborn mice. Sections were processed for Transglutaminase1 (TGM1) activity assay or negative Ctr (mutated TGM substrate, pepQNK5). **g** Quantification of TGM1 intensity from data shown in **f**. Data are the mean of 27 fields of view from n=3 newborn

mice per condition. Horizontal bars represent the mean intensity, and circles represent individual microscopy fields. ****P<0.0001 with Kolmogorov-Smirnov. **h** Dye exclusion assay. *shCtr* and *shSptan1 0595* transduced E17.5 embryos were treated with toluidine blue dye to evaluate the skin barrier.

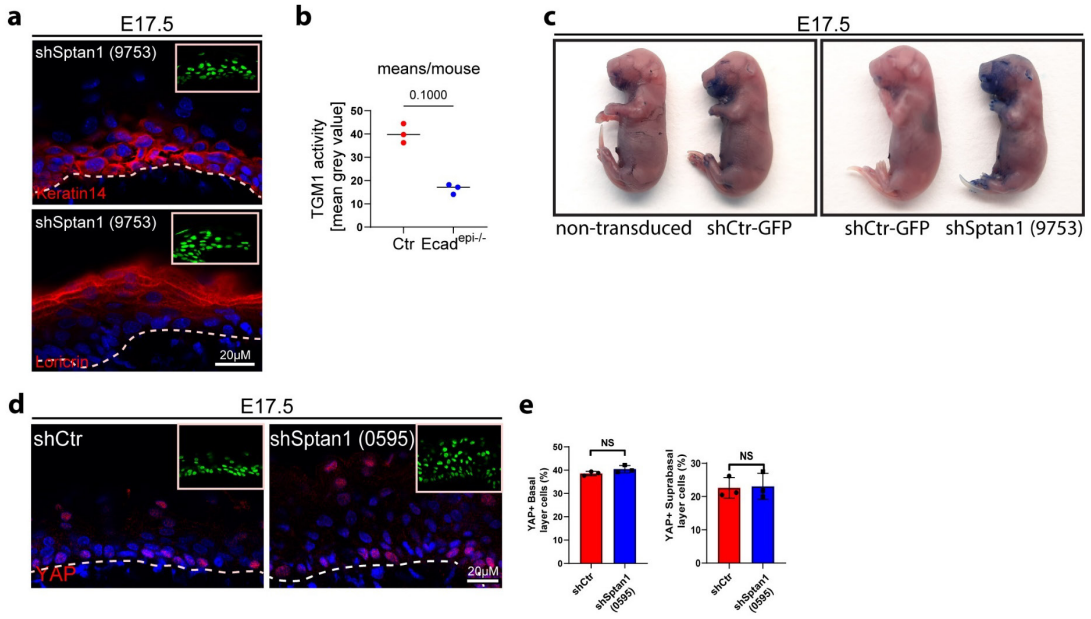

Supplementary Figure 4 αII-spectrin regulates epidermal differentiation and barrier function. **a** Sagittal views of 10-µm sections of dorsal skin from *shSptan1 9753* transduced E17.5 embryos immunolabeled for the basal layer marker K14 and the granular layer marker loricrin. Insets show the transduced cells (H2B−GFP+). **b** Quantification of TGM1 intensity from data shown in **Fig. 1f**. Circles represent the mean intensity per mouse of n=3 newborn mice per condition. P=0.1 with Mann-Whitney. **c** Dye exclusion assay. *shScr* (shCtr) and *shSptan1 9753* transduced E17.5 embryos were treated with toluidine blue dye to evaluate the skin barrier. **d** Sagittal views of 10-µm sections of dorsal skin from *shScr* (shCtr), and *shSptan1 0595* transduced E17.5 embryos immunolabeled for YAP. Insets show the transduced cells (H2B−GFP+). **e** Quantification of YAP+ nuclei in the basal (left) and suprabasal (right) layer cells from the data shown in **d**. Horizontal bars represent the mean ± SD from n=3 embryos per condition. Circles represent the average YAP+ nuclei of basal layer cells from each embryo. NS: P=0.1722 (basal), NS: P=0.883 (suprabasal) by unpaired t-test. Nuclei were stained with DAPI, and dotted lines indicate the dermal-epidermal border. Scale bars = 20 µm. NS, not significant.

αII-spectrin is required for the activity of the EGFR-TRPV3- TGM pathway.

We previously showed that E-cadherin controls the localization and activation of epidermal growth factor receptor (EGFR) during epidermal development, which is essential for the formation of a functional barrier (Rübsam et al., 2017). Furthermore, Cheng et al. showed that epidermal barrier formation requires the activation of both EGFR and the calcium channel TRPV3, which then activates the enzyme TGM (Cheng et al., 2010). Because spectrin functions as a structural platform that affects the organization of membrane domains and the activity of membrane proteins (Machnicka et al., 2014), we hypothesized that αII-spectrin promotes TGM by regulating the EGFR-TRPV3 pathway. To test this hypothesis, we first stained back skin from E17.5 control and *Sptan1* KD embryos for EGFR and phosphorylated EGFR (pEGFR) that indicates active EGFR. In both control and *Sptan1* KD embryos, we detected EGFR in all epidermal layers, with, as expected, the highest levels in the basal layer (Suppl. Fig. 5a). In control embryos, low levels of pEGFR were detected at the basal and spinous layers, and high levels of pEGFR were detected at the cortex of granular layer cells. However, In the *Sptan1*KD epidermis, this pattern was lost. Instead, pEGFR staining was diffuse or absent in many granular layer cells. In contrast, abnormally strong cortical staining was often detected in spinous layer cells (Fig. 5a). Quantifying pEGFR levels identified a significant 30% decrease in pEGFR levels in the granular layer and a 4-fold increase in the number of spinous cells exhibiting increased cortical pEGFR localization (Fig. 5b,c).

To determine whether αII-spectrin affects TRPV3 localization in the developing epidermis, we infected E9 embryos with lentivirus that harbors TRPV3-GFP (Xiao et al., 2008), and either *shScr* or *shSptan1* (*shScr; TRPV3-GFP* [control] and *shSptan1; TRPV3-GFP* [*Sptan1* KD] viruses) and analyzed TRPV3-GFP localization at E17.5 embryos. In the control epidermis, TRPV3-GFP was diffuse at the basal and spinous layers and cortical in the granular layer (Fig. 5d) where it was co-localized with pEGFR (Supplementary Fig. 5b). In contrast, in *Sptan1* KD embryos, a diffuse pattern of TRPV-GFP was detected in all the epidermal layers, including the granular layer (Fig. 5d; Supplementary Fig. 5c). IF quantification showed a 50% reduction of cortical TRPV3-GFP enrichment in *Sptan1*-depleted granular layer compared to control (Fig. 5e).

αII-spectrin-actomyosin networks regulate the actomyosin cytoskeleton

Our findings thus far reveal that αII-spectrin activity enhances epidermal barrier formation by regulating the EGFR-TRPV3-TGM pathway. Given that spectrin plays a critical role in the structural organization and mechanics of the cortical cytoskeleton, we asked whether αII-spectrin's regulation of the EGFR-TRPV3-TGM pathway is linked to its interaction with the actomyosin cytoskeleton. To this end, we treated WT E17.5 embryos with DMSO (control), latrunculin, and Y27632 to decrease F-actin levels and myosin II

motor activity. Similar to αII-spectrin KD epidermis, latrunculin, and Y27632 treatments decreased pEGFR levels in the granular layer by 15 and 23%, respectively, and increased cortical pEGFR levels in the spinous layer by 4- and 7-fold relative to DMSO-treated embryos (Fig. 5f-h). Importantly, in *shScr; TRPV3-GFP* transduced embryos treated with either latrunculin or Y27632 the cortical enrichment of TRPV3-GFP decreased by more than 50% compared to DMSO treatment (Fig. 5i,j). Moreover, latrunculin and Y27632 treatments decreased TGM activity by ~11%, and the cortical enrichment of the TGM activity signal decreased by ~40% (Fig. 5k,l,m). Together, the results presented here demonstrate that downstream to E-cadherin, spectrin governs the organization and mechanics of the cortical cytoskeleton, which, in turn, regulates both cell shape and signaling cascades required for epidermal barrier formation.

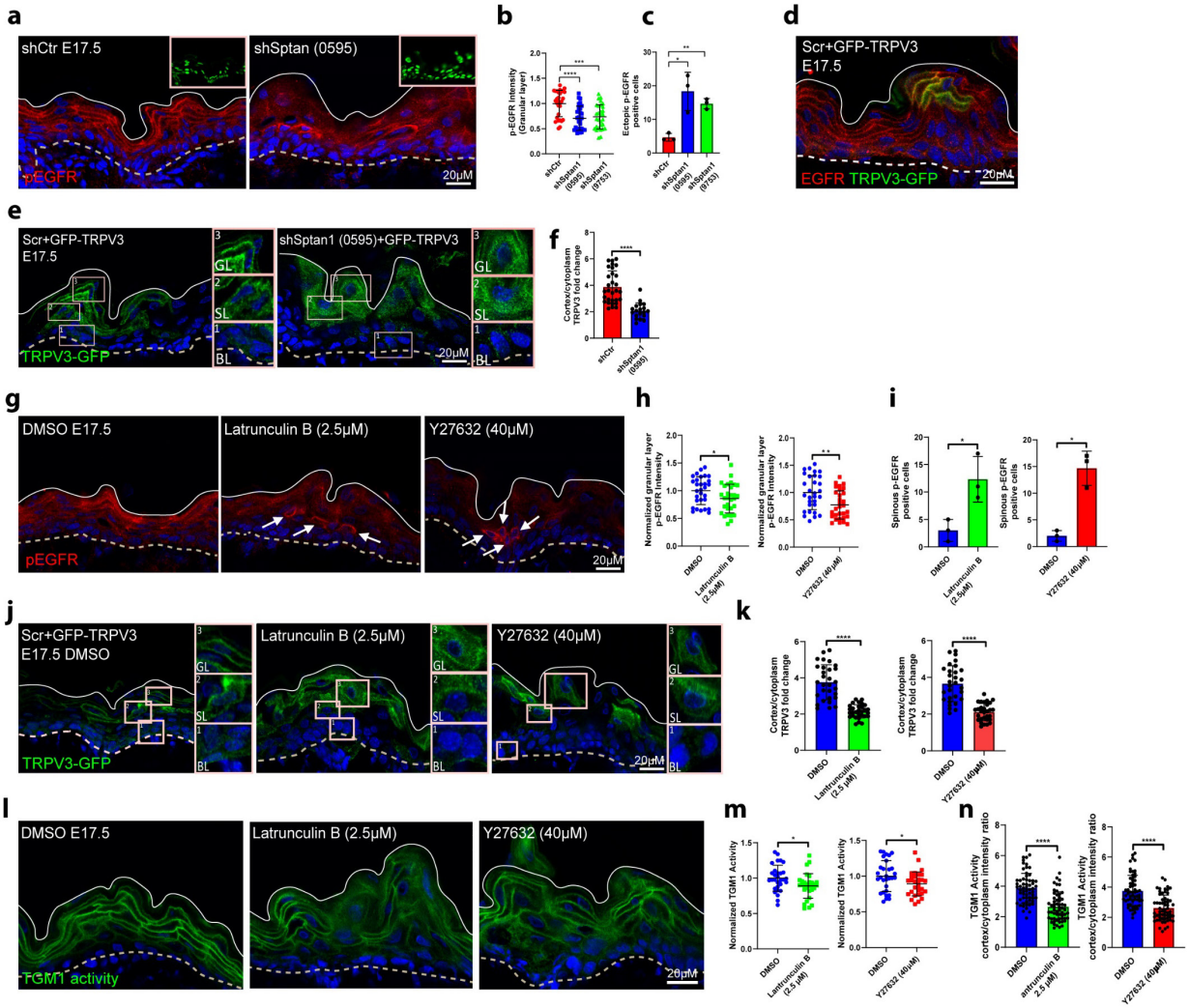

Figure 5 High-tension Actin-spectrin cortices recruit EGFR/TRPV3 to the plasma membrane. **a** Sagittal views of 10-µm sections of dorsal skin from *shScr* (*Ctr*), and *shSptan1 0595* transduced E17.5 embryos immunolabeled for pEGFR. Upper Insets show the transduced cells (H2B−GFP+). arrows show ectopic pEGFR-positive cells. **b** Quantification of pEGFR granular layer intensity from data shown in **a**. Data are the mean ± SD of 30 ROI (Region of interest) from n=3 embryos per condition. Horizontal bars represent the mean normalized intensity, and circles/squares/triangles represent individual microscopy fields. ****P<0.0001, ***P=0.0001 by unpaired t-test. **c** Quantification of ectopic pEGFR-positive cells from data shown in **a**. Horizontal bars represent the mean ± SD from n=3 embryos per condition. Circles represent the average ectopic pEGFR-positive cells from each embryo. *P=0.0482, **P=0.0011 by unpaired t-test. **d** Sagittal views of 10-µm sections of dorsal skin from *shScr;* TRPV3-GFP and *shSptan1 0595*; TRPV3-GFP transduced E17.5 embryos. Insets (right) show the magnification of the boxed area from each epidermal layer**. e** Quantification of TRPV3-GFP cortical enrichment from the data shown in **d**. Data are the mean ± SD from 30 individual cells from n=3 embryos per condition. Horizontal bars represent the TRPV3-GFP cortex/cytoplasm intensity ration mean and circles represent individual cells. ****P<0.0001 by unpaired t-test. **f** Sagittal views of 10-µm dorsal skin sections from E17.5 wild-type embryos treated with DMSO, latrunculin, or Y27632 immunolabeled for p-EGFR (Red). **g** Quantification of pEGFR granular layer intensity from data shown in **f**. Data are the mean ± SD of 30 ROI (Region of interest) from n=3 embryos per condition. Horizontal bars represent the mean normalized intensity, and circles/squares represent individual microscopy fields. *P=0.0345 (Latrunculin B), **P=0.0035 (Y27632) unpaired t-test. **h** Quantification of ectopic pEGFR-positive cells from data shown in **f**. Horizontal bars represent the mean ± SD from n=3 embryos per condition. Circles represent the average ectopic pEGFR-positive cells from each embryo. *P=0.0422 (Latrunculin B), *P=0.0143 (Y27632) by unpaired t-test. **i** Sagittal views of 10-µm sections of dorsal skin

from *shScr;* TRPV3-GFP transduced E17.5 embryos treated with DMSO, latrunculin or Y27632. Insets show the magnification of the boxed area from each epidermal layer. **j** Quantification of TRPV3-GFP cortical enrichment from the data shown in **i**. Data are the mean ± SD from 30 individual cells from n=3 embryos per condition. Horizontal bars represent the TRPV3-GFP cortex/cytoplasm intensity ration mean and circles represent individual cells. ****P <0.0001 by unpaired t-test. **k** Sagittal views of 10-µm dorsal skin sections from E17.5 wild-type embryos treated with DMSO, latrunculin and Y27632. Sections were processed for Transglutaminase1 (TGM1) activity assay. **i** Quantification of TGM1 intensity from data shown in **k**. Data are the mean ± SD of 30 ROI (Region of interest) from n=3 embryos per condition. Horizontal bars represent the mean normalized intensity, and circles/squares represent individual microscopy fields. *P=0.0205 (Latrunculin B), *P=0.0345 (Y27632) by unpaired t-test. **m** Quantification of TGM1 activity cortical enrichment from the data shown in **k**. Data are the mean ± SD from 60 individual cells from n=3 embryos per condition. Horizontal bars represent the TGM1 activity cortex/cytoplasm intensity ration mean and circles represent individual cells. ****P<0.0001 by unpaired t-test. Nuclei were stained with DAPI; dotted lines indicate the dermal-epidermal border. Scale bars = 20 µm. BL, Basal layer; SL, Spinous layer; GL, Granular layer.

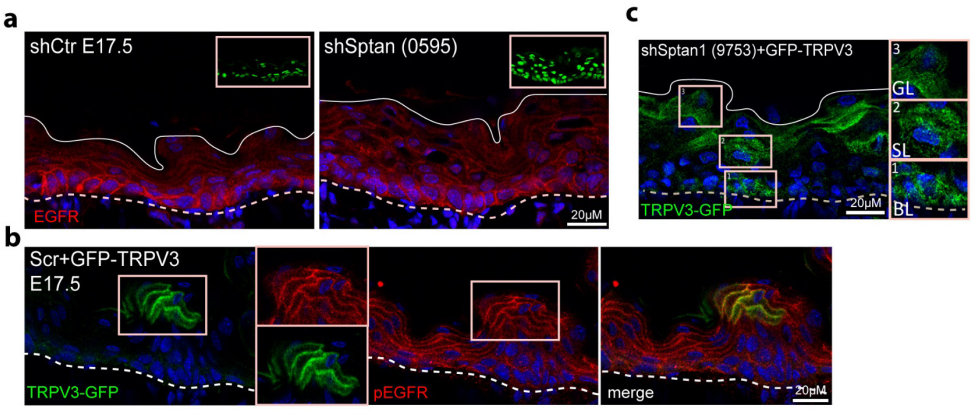

Supplementary Figure 5 High-tension Actin-spectrin cortices recruit EGFR/TRPV3 to the plasma membrane. **a** Sagittal views of 10-µm sections of dorsal skin from *shScr* (*Ctr*), and *shSptan1 0595* transduced E17.5 embryos immunolabeled for EGFR. Upper Insets show the transduced cells (H2B−GFP+). **b** Sagittal views of 10-µm sections of dorsal skin from *shScr;* TRPV3-GFP transduced E17.5 embryos immunolabeled for pEGFR. Insets (middle) show the magnification of boxed areas. **(C)** Sagittal views of 10-µm sections of dorsal skin from *shSptan1 9753*; TRPV3-GFP transduced E17.5 embryos. Insets (right) show the magnification of the boxed area from each epidermal layer**.** Nuclei were stained with DAPI.

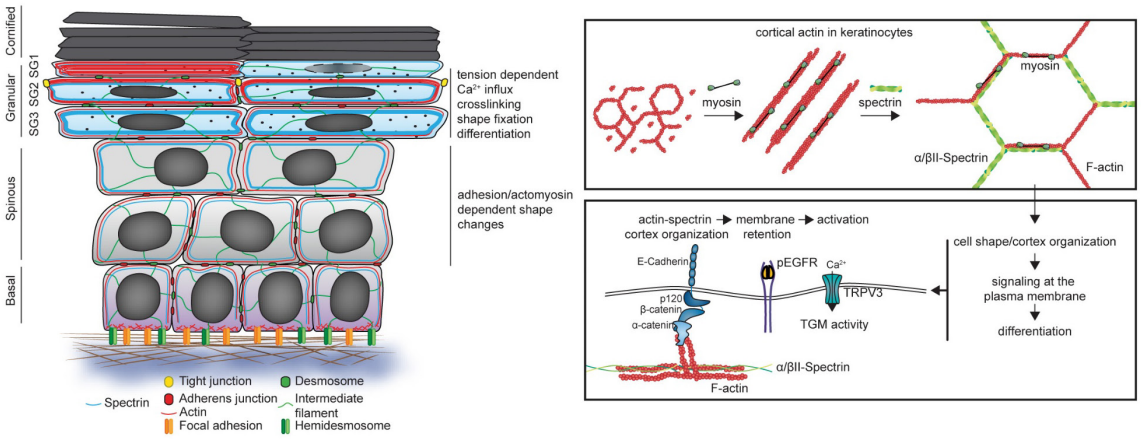

Figure 6 Model - High-tension actin-spectrin cortices regulate transglutaminase activity. Model of actin-spectrin dependent regulation of epidermal differentiation.

Discussion

In 1858, physician Rudolf Virchow established a correlation between cell shape and function, describing how abnormalities in cell shape can lead to disease development (Virchow, 1999). While the regulation of cell shape is a well-studied process dependent on adhesion and actomyosin, the mechanisms by which these processes also regulate differentiation and function require further elucidation. This study demonstrates that the E-cadherin-dependent integration of αII-spectrin into cortical actomyosin networks is crucial. This integration not only organizes the actomyosin network to control cell shape and mechanical robustness of the cortex, but it is also essential for differentiation and tissue barrier function.

The layered structure of the epidermis provides a unique example of the correlation between cell position, shape, and function, i.e., differentiation and barrier function (Peskoller et al., 2022; Luxenburg and Zaidel-Bar, 2019). Previously, we demonstrated that E-cadherin, a master regulator of cell-cell adhesion, is a key regulator of actomyosin-dependent tension, which controls the localization and activation of EGFR, essential for TJ barrier function in the epidermis (Rübsam et al., 2017). However, the precise mechanisms by which E-cadherin controls and localizes actomyosin tension were unclear. In this study, we show that E-cadherin regulates the differentiation-dependent cortical recruitment of αII-spectrin, organizing F-actin into a micro honeycomb-like lattice at the junctional interfaces of suprabasal cells. This reorganization controls cell shape changes that guide differentiation and provides mechanical resilience to the tensile actomyosin cortex. Simultaneously, this E-cadherin-linked spectrin-actin cortical network determines the localization and activation of EGFR/TRPV3 Ca^{2+} channel complexes, controlling the spatiotemporal activation of TGM essential for terminal differentiation and epidermal barrier function. Our data thus link cell shape, cell adhesion, and position-dependent cytoskeletal configuration to the spatial regulation of cell function, namely barrier formation.

Two mechanisms involving the actin cytoskeleton and cell shape changes have been shown to control early differentiation. First, mitotic rounding is crucial for regulated spindle orientation, which determines the position and fate of daughter cells (Luxenburg et al., 2011). Second, the compression of neighboring cells reduces their cortical tension and adhesion to the basement membrane, thereby promoting delamination and differentiation, with myosin IIa regulating early differentiation (Miroshnikova et al., 2018; Le et al., 2016). While these studies focused on basal layer cell shape changes, the present study demonstrates that changes in cortical spectrin-actin organization, which drives suprabasal cell shape, also regulate terminal differentiation, thereby establishing a direct correlation. We also show that in the developing epidermis, the initial suprabasal cortical enrichment of αII-spectrin coincides with suprabasal cell shape changes and differentiation (Supplementary Fig. 2b)(Moreci and Lechler, 2020; Roberts and Horsley, 2014; Koster and Roop, 2007). In the absence of αII-spectrin, defects in suprabasal actomyosin can explain reduced compaction and the diminished cortical localization of pEGFR and TRPV3 Ca^{2+} channels.

The precise mechanisms by which the spectrin-actomyosin network controls the cortical localization and activation of EGFR and TRPV3 remain to be elucidated. It has been suggested that EGFR stabilization at the plasma membrane may be facilitated either through cortical actomyosin interactions (Cole et al., 2008; Curto et al., 2007; Sullivan et al.; Chiasson-MacKenzie et al., 2015; Rübsam et al., 2017) or through interactions with αII-spectrin (Perez Verdaguer et al., 2022; Van Gelder et al.). Our in vivo data clearly demonstrate that cortical localization of pEGFR depends on an intact spectrin-actomyosin network.

Disruption of F-actin, myosin activity, or αII-spectrin results in the loss of cortical pEGFR (Fig. 4c-e, Fig. 5). Notably, the spectrin-actomyosin network specifically controls the cortical localization of active pEGFR (Fig. 5), which is necessary for the activation of TRPV3 channels (Cheng et al., 2010). These findings suggest that the spectrin-dependent organization of cortical actomyosin governs EGFR activity, thereby facilitating the formation of pEGFR-TRPV3 complexes in the granular layer.

In the epidermis, EGFR may play a dual role in barrier formation, both as part of TRPV3 complexes and at TJs (Cheng et al., 2010; Rübsam et al., 2017). It remains to be determined whether EGFR-dependent regulation of TJs and terminal differentiation are facets of the same mechanical regulation or are regulated through distinct mechanisms. Previous studies have shown that the loss of myosin IIa/b in the epidermis impairs TJ barrier function but does not affect stratum corneum barrier function (Sumigray et al., 2012) Conversely, impaired F-actin organization due to the loss of ArpC3 affects both barriers (Zhou et al., 2013). These observations demonstrate the profound complexity of the actomyosin cytoskeleton and the importance of its fine-tuning for the execution of distinct biological processes.

In conclusion, our data suggest a model in which E-cadherin-dependent cortical recruitment of αII-spectrin through regulation of actomyosin organization determines cell shape and promotes localization of pEGFR-TRPV3 complexes at the plasma membrane to activate TGM-dependent crosslinking in the granular-layer, thereby fixing cell shapes and promoting stratum corneum barrier function.

Materials and Methods

Mice

To generate E-cadherin$^{epi-/-}$ BL/6N mice, female E-cadherin$^{flox/flox}$ mice were crossed to male E-adherin$^{flox/wt}$;K14-Cre mice. Transgenic E-cadherin$^{flox/flox}$ mice and K14-Cre mice and their genotyping were described previously (Hafner et al., 2004; Boussadia et al., 2002). Hsd:ICR (CD1) mice (Envigo) were used for all in vivo knockdown experiments.

Isolation and culture of primary keratinocytes

Primary keratinocytes were isolated and cultured as described before (Rübsam et al., 2017): newborn mice were decapitated and incubated in 50% betaisodona/PBS for 30min at 4°C, 1 min PBS, 1 min 70% EtOH, 1min PBS and 1 min antibiotic/antimycotic solution. Skin was incubated in 2ml dispase (5 mg ml^{-1} in culture medium) solution. After incubation over night at 4 °C, skin was transferred onto 500 µl FAD medium on a 6 cm dish and epidermis was separated from the dermis as a sheet. Epidermis was transferred dermal side down onto 500 µl of TrypLE (Thermo Fisher Scientific) and incubated for 20 min at RT. Keratinocytes were washed out of the epidermal sheet using 3 ml of 10% FCS/PBS. After centrifugation keratinocytes were resuspended in FAD medium and seeded onto collagen type-1 (0.04 mg ml^{-1}) (Biochrom, L7213) coated cell culture plates. Primary murine keratinocytes were kept at 32 °C and 5% CO_2.
Primary keratinocytes were cultured in DMEM/HAM's F12 (FAD) medium with low Ca^{2+} (50 µM) (Biochrom) supplemented with 10% FCS (chelated), penicillin (100 U ml^{-1}), streptomycin (100 µg ml^{-1}, Biochrom A2212), adenine (1.8×10^{-4} M, SIGMA A3159), L-glutamine (2 mM, Biochrom K0282), hydrocortisone (0.5 µg ml^{-1}, Sigma H4001), EGF (10 ng ml^{-1}, Sigma E9644), cholera enterotoxin (0.1 nM, Sigma C-8052), insulin (5 µg ml^{-1}, Sigma I1882), and ascorbic acid (0.05 mg ml^{-1}, Sigma A4034).

Transfection

Overexpression: Keratinocytes were transfected at 100% confluency with Viromer®Red. 1.5 µg DNA were diluted in 100 µl Buffer E, added to 1.25 µl Viromer®RED and incubated for 15 min at RT (Rübsam et al., 2017). 33 µl transfection mix were used per well with 0.5 ml FAD medium (24 well plate). Knockdown: Keratinocytes were transfected at 100% confluency with Viromer®BLUE (lipocalyx; Halle Germany). Transfection mix was prepared according the manufacturers protocol. 100 µl transfection mix was used per well with 1 ml FAD medium (12 well plate, 5 nM siRNA f.c.). siRNA (siPOOLs) against αII-Spectrin were obtained from (siPOOLs from siTOOLs, Planegg, Germany).

Lentiviruses

Lentiviruses were produced as previously described (Beronja et al., 2010; Soffer et al., 2022). Briefly, lentiviral plasmids were generated by cloning oligonucleotides into pLKO.1-TRC (gift from David Root, Broad Institute, Cambridge, MA, USA; Addgene plasmid #10878), lentivirus-GFP or lentivirus-RFP (gift from Elaine Fuchs, Rockefeller University, New York, NY, USA; Addgene plasmid #25999) by digestion with EcoRI and AgeI, as described in the Genetic Perturbation Platform (GPP) website (http://portals.broadinstitute.org/gpp/public/resources/protocols). shRNA sequences were obtained from GPP (https://portals.broadinstitute.org/gpp/public/): Sptan1(0595) construct #TRCN0000090595, target sequence 5'- GCCACCGATGAAGCTTATAAA -3'. Sptan1(9753) construct #TRCN0000089753, target sequence 5'- CCAGTCACAATCACCAATGTT -3'. Ank3(6780) construct #TRCN0000236780, target sequence 5'- TGCCGTGGTTTCCCGGATTAA -3'. The TRPV3-GFP construct was a gift from Michael X. Zhu (UTHelath Houston).

In-utero lentivirus injection

Lentiviruses were injected into gestating mice as previously described (Beronja et al., 2010). Briefly, females at E8.5 were anesthetized with isoflurane, injected with pain killer, Rheumocam Veterinary 5 mg/ml according to the manufacturer instructions (Chanelle Pharma, Irland) and each embryo (up to 6 per litter) was injected with 0.4 to 1 µl of approximately 2×10^9 colony-forming units (CFUs) of the appropriate lentivirus. Controls were both uninfected littermates of *shSptan1-0595/9753*;H2B-GFP/*shSptan1-0595*;H2B-RFP/*shAnk3-6780*;H2B-GFP lentivirus-injected embryos and *shScr*;H2B-GFP lentivirus-injected embryos. For *shSptan1-0595/9753; TRPV3-GFP* lentivirus-injected embryos *shScr; TRPV3-GFP* were controls. In utero lentivirus injection infects approximately 60% to 70% of the dorsal skin epidermis (Beronja et al., 2010).

Immunofluorescence of keratinocytes in vitro

Immunofluorescence stainings of keratinocytes were performed as described before (Sahu et al., 2020a): cells were seeded on collagen coated glass cover slips in a 24 well plate and switched to high Ca^{2+} medium as indicated in the results section. Cells were fixed using 4% PFA for 10 minutes at RT, washed three times for 5 minutes using PBS, permeabilized using 0.5% TritonX100/PBS and blocked using 5% NGS/1% BSA/PBS for 1 hour at room temperature. Primary antibodies were diluted as indicated in the antibody section in Background Reducing Antibody Diluent Solution (ADS)(DAKO). Cover slips were placed growth surface down onto a 50 ml drop of staining solution on parafilm in a humidified chamber and incubated overnight at 4 °C. Cover slips were washed again with PBS three times for 10 minutes. Secondary antibodies and DAPI (40,6-diamidin-2-phenylindol, Sigma) were diluted 1:500 in ADS and cover slips were incubated for 1 hour at RT. Secondary antibodies were washed off via three wash steps using PBS for 10 minutes. Cover slips were mounted using Mowiol (Calbiochem).

Immunofluorescence on tissue sections

Embryos or newborn mice were embedded in OCT (Scigen), frozen, sectioned at 10 µM and fixed in 4% formaldehyde for 10 min. Sections were then blocked with 0.1% Triton X-100, 1% bovine serum albumin, 5% normal donkey serum in phosphate-buffered saline, or in MOM Basic kit reagent (Vector Laboratories). Sections were incubated with primary antibodies overnight at 4°C and with secondary antibodies for 1 h at room temperature.

Antibodies and inhibitors

Ankyrin3 (IF 1:500, WB 1:1000, Proteintech #27766-1-AP); **E-cadherin** (IF 1:200, BD Transduction Laboratories #610182, clone number 36 or IF 1:500, Cell Signaling #3195); **EGFR** (IF 1:500, Abcam #ab52894); pEGFR (Y1068)(IF 1:500, Abcam #ab40815); **GAPDH** (WB 1:10000, Ambion #AM4300 or WB 1:1000, Cell Signaling #5174); **GFP** (1:3000, Abcam #ab13970); **Keratin10** (IF 1:1000, BioLegend #PRB-159P); **Keratin14** (IF 1:2000, Covance #PRB 155P); **Loricrin** (1:1000, BioLegend #Poly19051); **phospho-Myosin Light Chain 2** (Thr18/Ser19) (IF 1:100, Cell Signaling #3674); **occludin** (IF 1:400, Invitrogen #33-1500); **TRPV3** (IF 1:1000, Abcam #b94582); **αII-Spectrin** (IF 1:500, WB 1:1000, Abcam ab11755); **α-catenin** (IF 1:2000, Sigma #C2081); **β-catenin** (IF 1:1000, Abcam #ab32572); **YAP** (IF 1:500, Cell Signaling #14074). **Phalloidin** was used to stain F-actin (IF 1:500, Sigma #P1951, TRITC conjugated). Secondary antibodies were species-specific antibodies conjugated with either AlexaFluor 488, 594 or 647, used at a dilution of 1:500 for immunofluorescence (Molecular Probes, Life Technologies), or with horseradish peroxidase antibodies used at 1:5000 for immunoblotting (Bio-Rad Laboratories).

Inhibitors used in this study if not indicated otherwise: Blebbistatin myosin inhibitor, 5 µM (Sigma #B0560); Latrunculin B, 0.1 µM (Sigma L5288).

Preparation of epidermal whole mounts

Epidermal whole mounts were prepared as has been described previously (Rübsam et al., 2017). Backskin was prepared from newborn mice and subcutaneous fat was removed with curved tweezers. The epidermis was mechanically, carefully peeled off from the dermis with ultrafine curved tweezers thereby separating the basal from the suprabasal layers. During the whole procedure the basal side of the sheet was kept floating on PBS2+ (PBS supplemented with 0.5mM MgCl2 and 0.1mM CaCl2). Subsequently the epidermal sheet was fixed floating on 4% PFA on ice for 10 min, washed on PBS for 5 min and permeabilized with 0.5% TritonX100/PBS for 1 h at room temperature (RT). The permeabilized sheet was washed for 5 min on PBS and blocked with 10% FCS/PBS for 30 min/RT. For staining epidermal sheet were cut into ca. 5 × 5mm pieces. The SC of the epidermis is prone unspecific binding of ABs. Additionally it cannot be permeabilized to allow AB permeation. Thus, all following steps were performed incubating the sheet from the basal side leaving the SC side dry. Primary ABs were diluted either in AB diluent solution (Dako, S3022) and incubated over night at 4 °C. Secondary ABs including DAPI and Phalloidin were incubated for 2 h/RT. After each AB incubation the sheet was rinsed 3× with PBS and washed 3× for 10 min. Finally the stained sheet was mounted in 50 µl Mowiol.

Isolation of single Stratum Granular (SG) and Stratum Spinous (SS) cells

Dorsal back skin of newborn mice was excised (approx. 10mm x 10mm) and fat tissue was removed with fine curved forceps. The epidermis was mechanically, carefully peeled off from the dermis with ultrafine curved tweezers thereby separating the basal from the suprabasal layers. Subsequently, the suprabasal epidermis was floated on a 400 µL droplet of 44 µg/mL rETA (Staphylococcus aureus Exfoliative Toxin A)/1mM $CaCl_2$ and incubated in the humidifying chamber at 37°C for 35 min. ETA diffuses intercellularly up to the tight junctions in the SG2 and cuts desmogleins-1 thereby loosening intercellular connections below the SG2 (Matsui et al., 2021). Layers below the SG2 layer (SS-SG3) were then peeled from the SG-1/2-corneum layers. Both parts were then floated onto 500 µL droplets of 0.05% trypsin/0.48 mM EDTA and incubated in the humidifying chamber at 37°C for 30 min. After the trypsinization, SG-1/2 and SS-SG3 cells were dissociated from the epidermis by manual pipetting from stratum corneum or and transferred to a 1.5 mL Eppendorf tube. To neutralize, 1 mL of PBS++ was added to the trypsin solution containing SG and SS cells and centrifuged at 3000 rpm for 5 min at RT. For treatment, cells were resuspended in Dulbecco's Modified Eagle Medium (DMEM) (Gibco).

Cytoskeletal inhibitor treatment on isolated SG and SS cells

After isolation, cells were treated with 1 mL DMEM with or without Latrunculin B, 0.1 µM, shaking at 300 rpm for 1 hr at 37°C. After the treatment cells were washed with 1 mL of PBS++, centrifuged at 3000 rpm for 5 min at RT, and fixed with 4% PFA for 10 min at RT. Cells were permeabilized using 0.5% TritonX100/PBS for 10 min and washed with 500 µL of PBS++. Consecutively, cells were treated with Phalloidin-TRITC and Dapi for 30 min at RT. After the incubation, cells were centrifuged and mounted on coverslips with 30 µL of Mowiol.

Cytoskeletal inhibitor treatment on embryos

For *in vivo* Latrunculin and Y27632 treatments, wild-type embryos or *shScr; TRPV3-GFP* transduced embryos were collected on E17.5 with 2.5µM latrunculin (Sigma-Aldrich) or with 40µM Y27632 (Sigma-Aldrich) or DMSO in serum-free DMEM (Biological Industries) at 37°C for 1 h before embedding in OCT.

Transglutaminase (Tgm1) enzyme-substrate assay on cryosections

Cryosections were washed with PBS++ until the cryo tissue embedding compound Tissue-Tek O.C.T Compound (Sakura Finetek 4583) was removed. Then, sections were circled with a hydrophobic barrier marker pen (ReadyProbes™ - Thermo Fisher Scientific) and blocked with 10% NGS/PBS for 1 h at RT. Subsequently, sections were treated with and without Transglutaminase 1 (Tgm1) peptide substrate (pepK5: 5/6-FITC-Doa-YEQHKLPSSWPF-NH2/OH and K5pepQN: 5/6-FITC-Doa-YENHKLPSSWPF-NH2/OH, Intavis peptide services) for 30 min at RT in a humidified chamber and washed three times with PBS to remove the unspecific binding. Next, sections were fixed with 4% PFA for 5 min at RT and washed with PBS three times for 5 min. Section were mounted using mowiol.

Toluidine blue barrier assay

Epidermal barrier assay was performed as previously described (Hardman et al., 1998). Briefly, E17.5 embryos were collected and immersed in an ice-cold methanol gradient in water, taking 2 min per step (1–25%, 2–50%, 3–75%, 4–100% methanol) and then rehydrated using the reverse procedure. Embryos were immersed in 0.2% toluidine blue solution. Embryos were washed in PBS before image capture.

Microscopy

Confocal images were obtained with a Leica TCS SP8, equipped with gateable hybrid detectors (HyDs). Objectives used with this microscope: PlanApo 63x, 1.4 NA CS2. Images to be used for deconvolution were obtained at optimal resolution according to Nyquist. Alternatively, images were acquired with a Nikon C2+ laser-scanning confocal microscope using a 60x, 1.4NA oil or a 20x, 0.75NA air objective (Nikon). Epifluorescence images were obtained with a Leica DMI6000. Objectives used with this microscope: PlanApo 63x, 1.4 NA.

Laser ablation

Keratinocytes were seeded on glass-bottom dishes (Ibidi # 81158) in FAD low Ca^{2+} medium. At confluency, the medium was switched to a high Ca^{2+} medium for 48 h. 2 h prior to imaging, medium was changed to high Ca^{2+} medium containing 1 µM SiR-actin (Spirochrome #CY-SC001). For laser ablation, a spinning Disk microscope (UltaView VoX, Perkin Elmer) equipped with a 355 nM pulsed YAG laser (Rapp Opto Electronic) was used. Experiments were performed at 37°C and 5 % CO2 using a water immersion objective 60 x, 1.2 NA (Nikon). The apical area apical stratified cells was ablated by drawing a line of consistent length with 30-50% laser power transmission and 10 iterations using UGA-40 Software (BioMedical Instruments).

Transepithelial resistance measurement

A total of 5×10^5 keratinocytes were seeded on transwell filters (Corning (#3460), 0.4 µm pore size). Cells were allowed to settle and then switched to 1.8mM high Ca2+ medium. Formation of TER was measured over time using an automated cell monitoring system (cellZscope, nanoAnalytics).

Semiquantitative RT-PCR

RNA was extracted from samples using a Direct-zol RNA extraction kit (Zymo Research; R2060), and equal amounts of RNA were reverse transcribed using ProtoScript First Strand cDNA Synthesis Kit (New England Biolabs). Semiquantitative PCR was conducted using a StepOnePlus System (Thermo Fisher Scientific). Data are presented as mRNA levels of the gene of interest normalized to peptidylprolyl isomerase B (Ppib) mRNA levels. Primers used in this study: *Sptan1* Forward 5'- TCGACAAGGACAAGTCTGGC-3'; *Sptan1* Reverse 5'- AACAGGGCAAGCAGTGTAGG-3'; *Ank3* Forward 5'- CTGACGTTCACGAGGGAGTT-3'; *Ank3* Reverse 5'- TATCTAACGTGTCCGCTGCC -3'; *PPIB* Forward 5'- GTGAGCGCTTCCCAGATGAGA-3'; *PPIB* Reverse 5'- TGCCGGAGTCGACAATGATG-3'

Image quantification:

Quantification F-actin, αII-spectrin, pEGFR, Ankyrin3 and TGM1 substrate levels in embryos

Intensities from layers as indicated in the figures and legends was measured using the freehand selection tool (Image J) with a width of 5 pixels. All intensity measurements were determined by CTCF (Corrected Total Cell Florescence) = Integrated density- (Area X mean of fluorescence of background readings). Intensity levels in each layer were normalized according to controls.

Quantification of Cell shape in embryos

Embryos that were injected with lentiviruses encoding *shScr;H2B-GFP,shsptan1;H2B-GFP* and *shAnk3-6780;H2B-GFP* on E8.5 and littermates were harvested at E17.5 frozen in OCT, sectioned (10 µm), fixed, and incubated overnight with E-cadherin antibody (Cell Signaling Technology, 3195, 1:500) at 4°C followed by incubation with a secondary antibody and DAPI at room temperature for 1 h. Samples were imaged using confocal microscopy with a 60×/1.4 objective that generated optical sections of 0.49 µm. The cell area of basal and suprabasal layer cells was measured by the Freehand tool (Image J).

YAP+ cell quantification

The number of GFP+ and YAP+ cells was counted manually. The percentage of YAP+ cells was calculated as (number of YAP+GFP+ double-positive cells/total number of GFP+ cells) × 100 for basal and suprabasal layer.

Quantification of cortical enrichment

The mean gray value of the granular layer cells' cortical and cytoplasmic intensity levels were measured with the “wand tool” (ImageJ) with a width of 5 pixels. The ratio between the two means was calculated and referred to as the fold change.

Statistics and repeatability of experiments
The numbers of independent experiments and biological replicates performed for all experiments, *p* values and the statistical tests that were used are indicated in the figure legends.

Ethics declaration

All animal protocols in this study have been approved by either the animal experiment committee of LANUV, North Rhine-Westphalia, Germany or University Animal Care and Use Committee, confirmation number TAU-MD-IL-2206-162-4. All methods were carried out in accordance with relevant guidelines and regulations. The animal protocols and the reporting in this manuscript follow the recommendations in the ARRIVE guidelines.

Data availability

The authors declare that the data supporting the findings of this study are available within the paper and its Supplementary Information files. Additional data are available from the corresponding author upon reasonable request.

Author contributions

MR, CL, AS and CMN conceived of the study. MR, CL, AS, TM and CMN designed experiments. AS, AB and MR carried out experiments and analyzed data. MR, CL, AS and CMN wrote the manuscript. All authors provided intellectual input, vetted and approved the final manuscript.

Acknowledgements

We like to thank the CECAD imaging facility under supervision of Astrid Schauss. This work is supported by the Deutsche Forschungsgemeinschaft DFG, German Research Foundation: Germany´s Excellence Strategy – EXC 2030/CECAD – 390661388 (to CMN); CECAD project: CECAD Career-Promoting Grant for Senior Postdoctoral Scientists (to MR); SPP 1782 NI 1234/6-2 (to CMN); ISF grant number 145/23 (to CL). This work was carried out in partial fulfilment of the requirements for a Ph.D. degree for AS. from the Faculty of Medical & Health Sciences, Tel-Aviv University

Competing interests

The authors declare no competing interests.

References

Bennett, V., and J. Healy. 2009. Membrane domains based on ankyrin and spectrin associated with cell-cell interactions. *Cold Spring Harb Perspect Biol*. 1:a003012. doi:10.1101/cshperspect.a003012.

Bennett, V., and D.N. Lorenzo. 2016. An Adaptable Spectrin/Ankyrin-Based Mechanism for Long-Range Organization of Plasma Membranes in Vertebrate Tissues. *Curr Top Membr*. 77:143–84. doi:10.1016/bs.ctm.2015.10.001.

Beronja, S., G. Livshits, S. Williams, and E. Fuchs. 2010. Rapid functional dissection of genetic networks via tissue-specific transduction and RNAi in mouse embryos. *Nat Med*. 16. doi:10.1038/nm.2167.

Bodine, D.M., C.S. Birkenmeier, and J.E. Barker. 1984. Spectrin deficient inherited hemolytic anemias in the mouse: characterization by spectrin synthesis and mRNA activity in reticulocytes. *Cell*. 37:721–9. doi:10.1016/0092-8674(84)90408-2.

Boussadia, O., S. Kutsch, A. Hierholzer, V. Delmas, and R. Kemler. 2002. E-cadherin is a survival factor for the lactating mouse mammary gland. *Mech Dev*. 115:53–62.

Calderón, J.C., P. Bolaños, and C. Caputo. 2014. The excitation-contraction coupling mechanism in skeletal muscle. *Biophys Rev*. 6:133–160. doi:10.1007/s12551-013-0135-x.

Cheng, X., J. Jin, L. Hu, D. Shen, X. ping Dong, M.A. Samie, J. Knoff, B. Eisinger, M.L. Liu, S.M. Huang, M.J. Caterina, P. Dempsey, L.E. Michael, A.A. Dlugosz, N.C. Andrews, D.E. Clapham, and H. Xu. 2010. TRP channel regulates EGFR signaling in hair morphogenesis and skin barrier formation. *Cell*. 141:331–343. doi:10.1016/j.cell.2010.03.013.

Chiasson-MacKenzie, C., Z.S. Morris, Q. Baca, B. Morris, J.K. Coker, R. Mirchev, A.E. Jensen, T. Carey, S.L. Stott, D.E. Golan, and A.I. McClatchey. 2015. NF2/Merlin mediates contact-dependent inhibition of EGFR mobility and internalization via cortical actomyosin. *Journal of Cell Biology*. 211:391–405. doi:10.1083/jcb.201503081.

Cole, B.K., M. Curto, A.W. Chan, and A.I. McClatchey. 2008. Localization to the Cortical Cytoskeleton Is Necessary for Nf2/Merlin-Dependent Epidermal Growth Factor Receptor Silencing. *Mol Cell Biol*. 28:1274–1284. doi:10.1128/mcb.01139-07.

Curto, M., B.K. Cole, D. Lallemand, C.H. Liu, and A.I. McClatchey. 2007. Contact-dependent inhibition of EGFR signaling by Nf2/Merlin. *Journal of Cell Biology*. 177:893–903. doi:10.1083/jcb.200703010.

Delaporte, C., B. Dautreaux, A. Rouche, and M. Fardeau. 1990. Changes in surface morphology and basal lamina of cultured muscle cells from Duchenne muscular dystrophy patients. *J Neurol Sci*. 95:77–88. doi:10.1016/0022-510x(90)90118-7.

Deng, H., W. Wang, J. Yu, Y. Zheng, Y. Qing, and D. Pan. 2015. Spectrin regulates Hippo signaling by modulating cortical actomyosin activity. *Elife*. 4. doi:10.7554/eLife.06567.

Dor-On, E., S. Raviv, Y. Cohen, O. Adir, K. Padmanabhan, and C. Luxenburg. 2017. T-plastin is essential for basement membrane assembly and epidermal morphogenesis. *Sci Signal*. 10. doi:10.1126/scisignal.aal3154.

Eckert, R.L., M.T. Sturniolo, A.M. Broome, M. Ruse, and E.A. Rorke. 2005. Transglutaminase function in epidermis. *Journal of Investigative Dermatology*. 124:481–492. doi:10.1111/j.0022-202X.2005.23627.x.

Elgsaeter, A., B.T. Stokke, A. Mikkelsen, and D. Branton. 1986. The molecular basis of erythrocyte shape. *Science*. 234:1217–23. doi:10.1126/science.3775380.

Emery, A.E.H. 2002. The muscular dystrophies. *Lancet*. 359:687–95. doi:10.1016/S0140-6736(02)07815-7.

Fletcher, G.C., A. Elbediwy, I. Khanal, P.S. Ribeiro, N. Tapon, and B.J. Thompson. 2015. The Spectrin cytoskeleton regulates the Hippo signalling pathway. *EMBO J*. 34:940–954. doi:10.15252/embj.201489642.

Fuchs, E. 2007. Scratching the surface of skin development. *Nature*. 445:834–42. doi:10.1038/nature05659.

Gaetani, M., S. Mootien, S. Harper, P.G. Gallagher, and D.W. Speicher. 2008. Structural and functional effects of hereditary hemolytic anemia-associated point mutations in the alpha spectrin tetramer site. *Blood*. 111:5712–20. doi:10.1182/blood-2007-11-122457.

Van Gelder, C.A.G.H., W. Van Bergen, P.C. Van Breugel, and M. Altelaar. Complementing the EGFR dynamic interactome using live-cell proximity labeling. *bioRxiv*. doi:10.1101/2022.02.02.478771.

Hafner, M., J. Wenk, A. Nenci, M. Pasparakis, K. Scharffetter-Kochanek, N. Smyth, T. Peters, D. Kess, O. Holtkötter, P. Shephard, J.E. Kudlow, H. Smola, I. Haase, A. Schippers, T. Krieg, and W. Müller. 2004. Keratin 14 Cre Transgenic Mice Authenticate Keratin 14 as an Oocyte-Expressed Protein. *Genesis (United States)*. 38:176–181. doi:10.1002/gene.20016.

Hardman, M.J., P. Sisi, D.N. Banbury, and C. Byrne. 1998. Patterned acquisition of skin barrier function during development. 1552:1541–1552.

Kalluri, R., and R.A. Weinberg. 2009. Review series The basics of epithelial-mesenchymal transition. *J Clin Invest*. 119. doi:10.1172/JCI39104.

Van Der Kammen, R., J.-Y. Song, I. De Rink, H. Janssen, S. Madonna, C. Scarponi, C. Albanesi, W. Brugman, and M. Innocenti. 2017. Knockout of the Arp2/3 complex in epidermis causes a psoriasis-like disease hallmarked by hyperactivation of transcription factor Nrf2. doi:10.1242/dev.156323.

Kizhatil, K., J.Q. Davis, L. Davis, J. Hoffman, B.L.M. Hogan, and V. Bennett. 2007. Ankyrin-G is a molecular partner of E-cadherin in epithelial cells and early embryos. *Journal of Biological Chemistry*. 282:26552–26561. doi:10.1074/jbc.M703158200.

Koegel, H., L. Von Tobel, M. Schäfer, S. Alberti, E. Kremmer, C. Mauch, D. Hohl, X.-J. Wang, H.-D. Beer, W. Bloch, A. Nordheim, and S. Werner. 2009. Loss of serum response factor in keratinocytes results in hyperproliferative skin disease in mice. *J Clin Invest*. 119. doi:10.1172/JCI37771.

Kong, C., X. Qu, M. Liu, W. Xu, D. Chen, Y. Zhang, S. Zhang, F. Zhu, Z. Liu, J. Li, C. Huang, and C. Wang. 2023. Dynamic interactions between E-cadherin and Ankyrin-G mediate epithelial cell polarity maintenance. *Nat Commun*. 14:6860. doi:10.1038/s41467-023-42628-1.

Koster, M.I., and D.R. Roop. 2007. Mechanisms regulating epithelial stratification. *Annu Rev Cell Dev Biol*. 23:93–113. doi:10.1146/annurev.cellbio.23.090506.123357.

Kubo, A., K. Nagao, M. Yokouchi, H. Sasaki, and M. Amagai. 2009. External antigen uptake by Langerhans cells with reorganization of epidermal tight junction barriers. *Journal of Experimental Medicine*. 206:2937–2946. doi:10.1084/jem.20091527.

Le, H.Q., S. Ghatak, C.Y.C. Yeung, F. Tellkamp, C. Günschmann, C. Dieterich, A. Yeroslaviz, B. Habermann, A. Pombo, C.M. Niessen, and S.A. Wickström. 2016. Mechanical regulation of transcription controls Polycomb-mediated gene silencing during lineage commitment. *Nat Cell Biol*. 18:864–875. doi:10.1038/ncb3387.

Lee, J., A.A. Abdeen, K.L. Wycislo, T.M. Fan, and K.A. Kilian. 2016. Interfacial geometry dictates cancer cell tumorigenicity. doi:10.1038/NMAT4610.

Leterrier, C., and P.A. Pullarkat. 2022. Mechanical role of the submembrane spectrin scaffold in red blood cells and neurons. doi:10.1242/jcs.259356.

Luxenburg, C., D. Geblinger, E. Klein, K. Anderson, D. Hanein, B. Geiger, and L. Addadi. 2007. The architecture of the adhesive apparatus of cultured osteoclasts: from podosome formation to sealing zone assembly. *PLoS One*. 2:e179. doi:10.1371/journal.pone.0000179.

Luxenburg, C., E. Heller, H.A. Pasolli, S. Chai, M. Nikolova, N. Stokes, and E. Fuchs. 2015. Wdr1-mediated cell shape dynamics and cortical tension are essential for epidermal planar cell polarity. *Nat Cell Biol*. 17:592–604. doi:10.1038/ncb3146.

Luxenburg, C., H.A. Pasolli, S.E. Williams, and E. Fuchs. 2011. Developmental roles for Srf, cortical cytoskeleton and cell shape in epidermal spindle orientation. *Nature Publishing Group*. doi:10.1038/ncb2163.

Luxenburg, C., and R. Zaidel-Bar. 2019. From cell shape to cell fate via the cytoskeleton — Insights from the epidermis. *Exp Cell Res*. 378:232–237. doi:10.1016/j.yexcr.2019.03.016.

Machnicka, B., A. Czogalla, A. Hryniewicz-Jankowska, D.M. Bogusławska, R. Grochowalska, E. Heger, and A.F. Sikorski. 2014. Spectrins: a structural platform for stabilization and activation of membrane channels, receptors and transporters. *Biochim Biophys Acta*. 1838:620–34. doi:10.1016/j.bbamem.2013.05.002.

Machnicka, B., R. Grochowalska, D.M. Bogusławska, and A.F. Sikorski. 2019. The role of spectrin in cell adhesion and cell–cell contact. *Exp Biol Med*. 244:1303–1312. doi:10.1177/1535370219859003.

Mahly, A., K. Padmanabhan, A. Soffer, J. Cohen, J. Omar, R. Sagi-Eisenberg, and C. Luxenburg. 2022. Anillin governs mitotic rounding during early epidermal development. *BMC Biol*. 20:145. doi:10.1186/s12915-022-01345-9.

Matsui, T., N. Kadono-maekubo, Y. Suzuki, Y. Furuichi, and K. Shiraga. 2021. A unique mode of keratinocyte death requires intracellular acidification. 1–10. doi:10.1073/pnas.2020722118.

Miroshnikova, Y.A., H.Q. Le, D. Schneider, T. Thalheim, M. Rübsam, N. Bremicker, J. Polleux, N. Kamprad, M. Tarantola, I. Wang, M. Balland, C.M. Niessen, J. Galle, and S.A. Wickström. 2018. Adhesion

forces and cortical tension couple cell proliferation and differentiation to drive epidermal stratification. *Nat Cell Biol*. 20:69–80. doi:10.1038/s41556-017-0005-z.

Moreci, R.S., and T. Lechler. 2020. Epidermal structure and differentiation. *Current Biology*. 30:R144–R149. doi:10.1016/j.cub.2020.01.004.

Nelson, W.J., E.M. Shore, A.Z. Wang, and R.W. Hammerton. 1990. Identification of a membrane-cytoskeletal complex containing the cell adhesion molecule uvomorulin (E-cadherin), ankyrin, and fodrin in Madin-Darby canine kidney epithelial cells. *J Cell Biol*. 110:349–57. doi:10.1083/jcb.110.2.349.

Niessen, C.M., M.L. Manning, and S.A. Wickström. 2024. Mechanochemical Principles of Epidermal Tissue Dynamics. *Cold Spring Harb Perspect Biol*. doi:10.1101/cshperspect.a041518.

Noordstra, I., R.G. Morris, and A.S. Yap. 2023. Cadherins and the cortex: A matter of time? *Curr Opin Cell Biol*. 80:102154. doi:10.1016/j.ceb.2023.102154.

Padmanabhan, K., H. Grobe, J. Cohen, A. Soffer, A. Mahly, O. Adir, R. Zaidel-Bar, and C. Luxenburg. 2020. Thymosin β4 is essential for adherens junction stability and epidermal planar cell polarity. *Development*. 147. doi:10.1242/dev.193425.

Pan, L., R. Yan, W. Li, and K. Xu. 2018. Super-Resolution Microscopy Reveals the Native Ultrastructure of the Erythrocyte Cytoskeleton. *Cell Rep*. 22:1151–1158. doi:10.1016/j.celrep.2017.12.107.

PAULING, L., and H.A. ITANO. 1949. Sickle cell anemia a molecular disease. *Science*. 110:543–8. doi:10.1126/science.110.2865.543.

Perez Verdaguer, M., T. Zhang, S. Surve, J.A. Paulo, C. Wallace, S.C. Watkins, S.P. Gygi, and A. Sorkin. 2022. Time-resolved proximity labeling of protein networks associated with ligand-activated EGFR. *Cell Rep*. 39. doi:10.1016/j.celrep.2022.110950.

Peskoller, M., A. Bhosale, K. Göbel, J. Löhr, S. Miceli, S. Perot, O. Persa, M. Rübsam, J. Shah, H. Zhang, and C.M. Niessen. 2022. How to Build and Regenerate a Functional Skin Barrier: The Adhesive and Cell Shaping Travels of a Keratinocyte. *Journal of Investigative Dermatology*. 142. doi:10.1016/j.jid.2021.12.034.

Pollard, T.D. 2016. Actin and Actin-Binding Proteins. *Cold Spring Harb Perspect Biol*. 8. doi:10.1101/cshperspect.a018226.

Pradhan, D., C.R. Lombardo, S. Roe, D.L. Rimm, and J.S. Morrow. 2001. α-Catenin Binds Directly to Spectrin and Facilitates Spectrin-Membrane Assembly in Vivo. *Journal of Biological Chemistry*. 276:4175–4181. doi:10.1074/jbc.M009259200.

Roberts, N., and V. Horsley. 2014. Developing stratified epithelia: lessons from the epidermis and thymus. *WIREs Dev Biol*. 3:389–402. doi:10.1002/wdev.146.

Rübsam, M., A.F. Mertz, A. Kubo, S. Marg, C. Jüngst, G. Goranci-Buzhala, A.C. Schauss, V. Horsley, E.R. Dufresne, M. Moser, W. Ziegler, M. Amagai, S.A. Wickström, and C.M. Niessen. 2017. E-cadherin integrates mechanotransduction and EGFR signaling to control junctional tissue polarization and tight junction positioning. *Nat Commun*. 8:1–15. doi:10.1038/s41467-017-01170-7.

Saha, A., M. Nishikawa, M. Behrndt, C.P. Heisenberg, F. Jülicher, and S.W. Grill. 2016. Determining Physical Properties of the Cell Cortex. *Biophys J*. 110:1421–1429. doi:10.1016/j.bpj.2016.02.013.

Sahu, P., D.M. Sussman, M. Rübsam, A.F. Mertz, V. Horsley, E.R. Dufresne, C.M. Niessen, M.C. Marchetti, M.L. Manning, and J.M. Schwarz. 2020a. Small-scale demixing in confluent biological tissues. *Soft Matter*. 16:3325–3337. doi:10.1039/c9sm01084j.

Sahu, P., D.M. Sussman, M. Rübsam, A.F. Mertz, V. Horsley, E.R. Dufresne, C.M. Niessen, M.C. Marchetti, M.L. Manning, and J.M. Schwarz. 2020b. Small-scale demixing in confluent biological tissues. *Soft Matter*. 16:3325–3337. doi:10.1039/c9sm01084j.

Saitsu, H., J. Tohyama, T. Kumada, K. Egawa, K. Hamada, I. Okada, T. Mizuguchi, H. Osaka, R. Miyata, T. Furukawa, K. Haginoya, H. Hoshino, T. Goto, Y. Hachiya, T. Yamagata, S. Saitoh, T. Nagai, K. Nishiyama, A. Nishimura, N. Miyake, M. Komada, K. Hayashi, S.-I. Hirai, K. Ogata, M. Kato, A. Fukuda, and N. Matsumoto. 2010. Dominant-negative mutations in alpha-II spectrin cause West syndrome with severe cerebral hypomyelination, spastic quadriplegia, and developmental delay. *Am J Hum Genet*. 86:881–91. doi:10.1016/j.ajhg.2010.04.013.

Saraswathibhatla, A., D. Indana, and O. Chaudhuri. 2023. nature reviews molecular cell biology Cell-extracellular matrix mechanotransduction in 3D. *Nat Rev Mol Cell Biol*. 24:495–516. doi:10.1038/s41580-023-00583-1.

Sennett, R., Z. Wang, A. Rezza, L. Grisanti, N. Roitershtein, C. Sicchio, K.W. Mok, N.J. Heitman, C. Clavel, A. Ma'ayan, and M. Rendl. 2015. An Integrated Transcriptome Atlas of Embryonic Hair Follicle Progenitors, Their Niche, and the Developing Skin. *Dev Cell*. 34:577–591. doi:10.1016/j.devcel.2015.06.023.

Simpson, C.L., D.M. Patel, and K.J. Green. 2011a. Deconstructing the skin: cytoarchitectural determinants of epidermal morphogenesis. doi:10.1038/nrm3175.

Simpson, C.L., D.M. Patel, and K.J. Green. 2011b. Deconstructing the skin: cytoarchitectural determinants of epidermal morphogenesis. doi:10.1038/nrm3175.

Soffer, A., A. Mahly, K. Padmanabhan, J. Cohen, O. Adir, E. Loushi, Y. Fuchs, S.E. Williams, and C. Luxenburg. 2022. Apoptosis and tissue thinning contribute to symmetric cell division in the developing mouse epidermis in a nonautonomous way. *PLoS Biol*. 20. doi:10.1371/JOURNAL.PBIO.3001756.

Stankewich, M.C., C.D. Cianci, P.R. Stabach, L. Ji, A. Nath, and J.S. Morrow. 2011. Cell organization, growth, and neural and cardiac development require αII-spectrin. *J Cell Sci*. 124:3956–66. doi:10.1242/jcs.080374.

Sugimura, Y., M. Hosono, M. Kitamura, T. Tsuda, K. Yamanishi, M. Maki, and K. Hitomi. 2008. Identification of preferred substrate sequences for transglutaminase 1 – development of a novel peptide that can efficiently detect cross-linking enzyme activity in the skin. *FEBS J*. 275:5667–5677. doi:10.1111/j.1742-4658.2008.06692.x.

Sullivan, B., T. Light, V. Vu, A. Kapustka, K. Hristova, D. Leckband, and J. Brugge. Mechanical disruption of E-cadherin complexes with epidermal growth factor receptor actuates growth factor-dependent signaling. doi:10.1073/pnas.2100679119/-/DCSupplemental.

Sumigray, K.D., H.P. Foote, and T. Lechler. 2012. Noncentrosomal microtubules and type II myosins potentiate epidermal cell adhesion and barrier formation. *Journal of Cell Biology*. 199:513–525. doi:10.1083/jcb.201206143.

Teliska, L.H., and M.N. Rasband. 2021. Spectrins. *Curr Biol*. 31:R504–R506. doi:10.1016/j.cub.2021.01.040.

Thi Kim Vuong-Brender, T., M. Ben Amar, J. Pontabry, and M. Labouesse. The interplay of stiffness and force anisotropies drives embryo elongation. doi:10.7554/eLife.23866.001.

Tunggal, J.A., I. Helfrich, A. Schmitz, H. Schwarz, D. Günzel, M. Fromm, R. Kemler, T. Krieg, and C.M. Niessen. 2005. E-cadherin is essential for in vivo epidermal barrier function by regulating tight junctions. *EMBO Journal*. 24:1146–1156. doi:10.1038/sj.emboj.7600605.

Vasioukhin, V., C. Bauer, M. Yin, and E. Fuchs. 2000. Directed actin polymerization is the driving force for epithelial cell-cell adhesion. *Cell*. 100:209–219.

Virchow, R. 1999. Founder of Cellular Pathology. *Journal of Pelvic Surgery*. 5:175–177.

Wu, J., P.P. Masci, C. Chen, J. Chen, M.F. Lavin, and K.N. Zhao. 2015. β-Adducin siRNA disruption of the spectrin-based cytoskeleton in differentiating keratinocytes prevented by calcium acting through calmodulin/epidermal growth factor receptor/cadherin pathway. *Cell Signal*. 27:15–25. doi:10.1016/j.cellsig.2014.10.001.

Xiao, R., J. Tian, J. Tang, and M.X. Zhu. 2008. The TRPV3 mutation associated with the hairless phenotype in rodents is constitutively active. *Cell Calcium*. 43:334–343. doi:10.1016/j.ceca.2007.06.004.

Yokouchi, M., T. Atsugi, M. Van Logtestijn, and R.J. Tanaka. 2016. Epidermal cell turnover across tight junctions based on Kelvin ' s tetrakaidecahedron cell shape. 1–20. doi:10.7554/eLife.19593.

Yoshida, K., M. Yokouchi, K. Nagao, K. Ishii, M. Amagai, and A. Kubo. 2013. Functional tight junction barrier localizes in the second layer of the stratum granulosum of human epidermis. *J Dermatol Sci*. 71:89–99. doi:10.1016/j.jdermsci.2013.04.021.

Zaidel-Bar, R., G. Zhenhuan, and C. Luxenburg. 2015. The contractome-a systems view of actomyosin contractility in non-muscle cells. doi:10.1242/jcs.170068.

Zhao, K.-N., P.P. Masci, J. Chen, and M.F. Lavin. 2013. Calcium prevents retinoic acid-induced disruption of the spectrin-based cytoskeleton in keratinocytes through the Src/PI3K-p85α/AKT/PKCδ/β-adducin pathways. *Cell Calcium*. 54:151–62. doi:10.1016/j.ceca.2013.05.009.

Zhao, K.N., P.P. Masci, and M.F. Lavin. 2011. Disruption of spectrin-like cytoskeleton in differentiating keratinocytes by PKCδ activation is associated with phosphorylated adducin. *PLoS One*. 6. doi:10.1371/journal.pone.0028267.

Zhou, K., A. Muroyama, J. Underwood, R. Leylek, S. Ray, S.H. Soderling, and T. Lechler. 2013. Actin-related protein2/3 complex regulates tight junctions and terminal differentiation to promote epidermal barrier formation. *Proc Natl Acad Sci U S A*. 110. doi:10.1073/pnas.1308419110.